NeuroImage 187 (2019) 209–225

Contents lists available at ScienceDirect

NeuroImage

journal homepage: www.elsevier.com/locate/neuroimage

Functional MRI of brain physiology in aging and neurodegenerative diseases

J. Jean Chen [a,b,*]

[a] Rotman Research Institute at Baycrest Centre, Canada
[b] Department of Medical Biophysics, University of Toronto, Canada

ARTICLE INFO

Keywords:
Aging
Neurodegeneration
fMRI
Brain physiology
Dementia
Cerebrovascular health

ABSTRACT

Brain aging and associated neurodegeneration constitute a major societal challenge as well as one for the neuroimaging community. A full understanding of the physiological mechanisms underlying neurodegeneration still eludes medical researchers, fuelling the development of in vivo neuroimaging markers. Hence it is increasingly recognized that our understanding of neurodegenerative processes likely will depend upon the available information provided by imaging techniques. At the same time, the imaging techniques are often developed in response to the desire to observe certain physiological processes. In this context, functional MRI (fMRI), which has for decades provided information on neuronal activity, has evolved into a large family of techniques well suited for in vivo observations of brain physiology. Given the rapid technical advances in fMRI in recent years, this review aims to summarize the physiological basis of fMRI observations in healthy aging as well as in age-related neurodegeneration. This review focuses on in-vivo human brain imaging studies in this review and on disease features that can be imaged using fMRI methods. In addition to providing detailed literature summaries, this review also discusses future directions in the study of brain physiology using fMRI in the clinical setting.

Introduction

As the world population ages, the number of individuals affected by age-related neurodegenerative disorders is expected to rapidly increase. As an example, for Alzheimer's disease (AD), the prevalence is expected to double within the next 20 years (Prince et al., 2013). Neuroimaging has provided much valuable evidence of functional and structural changes that take place in aging and associated neurodegenerative diseases, and has an increasing capacity to provide unparalleled insight into the mechanisms that sustain the living human brain. Knowledge about brain physiology in aging and neurodegeneration hold the key to understanding the sources of the observed changes, and may indeed lead to early detection and halting of disease progression.

This review focuses on the measurement of brain physiology. In the medical context, "physiology" contrasts "anatomy" and pertain to the processes supporting brain function, mainly including vascular and metabolic function. This review will begin by summarizing the current understanding regarding the physiological mechanisms sustaining human brain function, to be followed by a summary of physiological metrics that can be measured using functional MRI (fMRI) techniques. The imaging work and findings are discussed with previous findings using well-established imaging and spectroscopic techniques.

Human brain physiology

The human brain constitutes fewer than 2% of the average body weight but consumes over 20% of the nutrients (Drubach, 2000). This energy-intensive organ requires a constant supply of nutrients to feed neuronal communications through neuronal firing and postsynaptic currents. The biochemical and vascular mechanisms underlying neuronal activity are detailed in the following subsections.

Neural activity and cerebral energetics

Action potentials, otherwise referred to as spikes or neuronal firing, trigger the influx of calcium ions (Ca^{2+}) and thus the release of neurotransmitter-filled vesicles across the synaptic cleft. The vesicles then bind with receptor molecules in the postsynaptic membrane. This binding, also called synapses, engenders small hyperpolarizing currents altering the membrane potential in the postsynaptic neuron, either giving rise to new action potentials (excitatory synapse) or preventing them (inhibitory synapse), thus realizing the extensive propagation of neuronal signalling. A neuron's ability to generate synaptic and action potentials depends on the existence of an electrochemical gradient across the cell membrane, arising from intra-extracellular differences in the

* Corresponding author. Rotman Research Institute, Baycrest, 3560 Bathurst Street Toronto, Ontario, M6A. 2E1, Canada.
E-mail address: jchen@research.baycrest.org.

https://doi.org/10.1016/j.neuroimage.2018.05.050
Received 26 September 2017; Received in revised form 16 May 2018; Accepted 20 May 2018
Available online 21 May 2018

concentrations of various ions, most notably sodium (Na^+) and potassium (K^+).

The propagation of both synaptic and action potentials is mediated by the opening of ion channels, and powered by adenosine triphosphate (ATP) molecules. The cellular ATP requirements are modulated by the rate of synapses and neuronal firing, and increases in the discharge frequency result in a greater need for glucose and oxygen, the basic substrates of ATP production. A main channel of ATP synthesis is through glycolysis, a series of anaerobic, enzyme-catalyzed reactions resulting in the conversion of glucose into ATP, pyruvate and lactate. Normally, glycolysis is followed by the *trans*-carboxylic acid cycle, a more efficient ATP synthesizing process that is associated with oxygen utilization in the mitochondria (oxidative phosphorylation), as well as CO2 and water as by-products. This reliance on O_2 and glucose constitutes the classic view of neuroenergetics, as the overwhelmingly superior efficiency of oxidative ATP production precludes the possibility of a purely anaerobic response to stimulation-driven ATP demand (Shulman et al., 2001). ATP production in the mitochondria also induces the formation of reactive oxygen species (ROS) that can be harmful for cells, as exemplified by the aging process.

Notwithstanding, stimulus-dependent variations in the oxygen-to-glucose metabolism ratio has been repeatedly reported using PET and MR spectroscopy (Marrett and Gjedde, 1997; Shulman et al., 2001), suggesting a transient utilization of a tissue glycogen reserve that is not account for in the classic view. This has been proposed as the result of lactate conversion into pyruvate in a non-oxidative process, though with much lower efficiency than oxidative phosphorylation (Gjedde et al., 2002). However, the fMRI techniques introduced in this review are mostly built upon blood-flow or blood-oxygenation based mechanisms, and thus target phenomenon consistent with O_2-glucose neuroenergetics.

Neurovascular coupling and the neurovascular unit

Traditionally it has been understood that surges in the brain's energy needs is met via increased tissue perfusion (CBF) (Roy and Sherrington, 1890), realized by dilation of the arterioles and retrogradely by the pial arteries (Duling and Berne, 1970), which decreases the resistance of the latter to flow and leads to increased blood volume (CBV) (Grubb et al., 1974). This process is referred to as *functional hyperemia*, which enhances not only nutrient transport but also waste removal and temperature regulation. This process, termed *neurovascular coupling*, is a fundamental component of cerebral homeostasis, and is accomplished by a group of cells known as the *neurovascular unit* (Fig. 1).

Initially, the hemodynamic response is thought to be initiated through contractions and relaxations of arterial smooth muscles (regulated globally and locally). This feedback-based control mechanism is responds to changes in energy demand, as ATP is required for re-establishing iron gradients after neuronal signalling (Attwell and Laughlin, 2001). The need for a hemodynamic response could be signalled through a lack of O_2 or glucose, or an increase in CO_2 production. This process has traditionally been associated solely with neuronal signalling, hence the term neurovascular coupling. The O2 supplied by the hemodynamic response far exceeds what appears to be required by neural activity, a phenomenon that has yet to be fully explained (Buxton and Frank, 1997; Hayashi et al., 2003; Leithner and Royl, 2013; Paulson et al., 2010).

As a side note, strong CBF responses can be induced by intravascular CO_2 alterations. Notwithstanding the nervous response initiation by the macrovascular CO_2 receptors, the homeostatic blood pH is actively maintained. Thus, hypercapnic challenges, in which the arterial CO_2 content is increased, inducing large CBF increases without a significant concomitant increase in metabolic rate (Chen and Pike, 2010; Jain et al., 2011), have been widely used to study cerebrovascular coupling. Regional flow variations can also be triggered by changes in extracellular K^+, Ca^{2+} and ATP concentrations (Lassen, 1991). In addition, much importance has been attached to the role of nitric oxide (NO), which is synthesized locally following glutamate receptor activity, and has been implicated in the modulation of vasodilatory effects produced by nearly all the above mediators (Iadecola et al., 1994).

Later studies involving blood O_2 and glucose manipulations pointed to an alternate neurovascular regulation mechanism, as it was clear that local CO_2 increases were not the main driver of functional hyperemia, which is instead mediated by a number of vasoactive and metabolic agents (Girouard and Iadecola, 2006). Notably, the synaptic release of glutamate activates neuronal NMDA (N-methyl-D-aspartate) receptors, resulting in the entry of Ca^{2+} into neurons and the release of the vasodilatory NO. However, NO concentration might simply mediate instead of govern neuron-vessel signalling (Akgören et al., 1996) (Yang et al., 2003). The glia and interneurons have also been implicated in what is considered a feed-forward vascular-control mechanism (Cauli et al., 2004).

The neuroglia, particularly astrocytes, have been implicated in feed-forward neurovascular coupling at the microvascular level through a number of pathways. ATP is not only taken up by the restoration of post-synaptic ionic gradients, but also in the astrocytes by excitatory amino acid transporters for glutamate-to-glutamine conversion, whereby

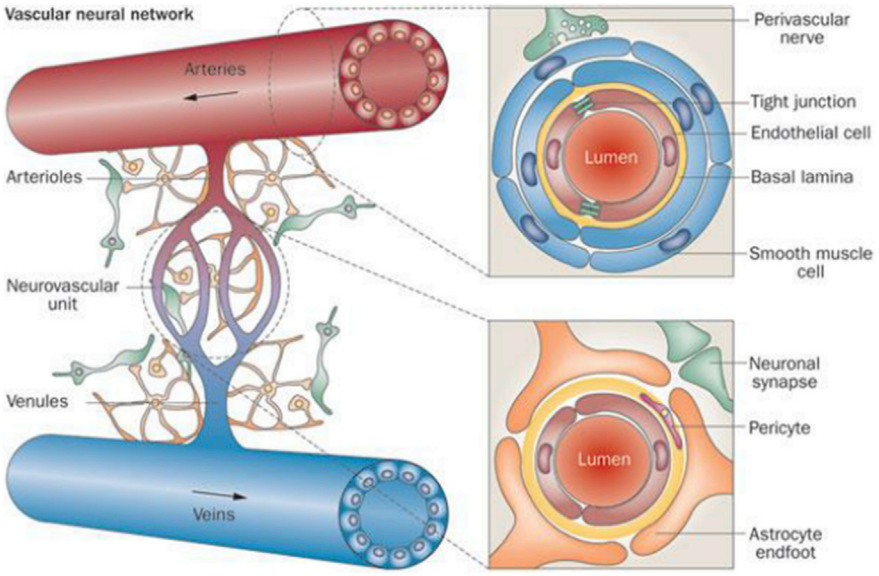

Fig. 1. The neurovascular unit and blood-brain barrier. The neurovascular unit consists of capillary endothelial cells, pericytes and basal lamina enveloped by astrocyte endfeet. Astrocytes communicate with adjacent neurons via metabolite exchange. Vascular endothelial cells are sealed by tight junctions that constitute the blood-brain barrier (BBB). The vascular neural network, therefore, comprises all cells and structures required to maintain cerebral blood flow under physiological and pathological conditions. Figure is reproduced from (Zhang et al., 2012) with permission.

glutamate is a main excitatory neurotransmitter that must be recycled into glutamine for uptake by neurons. This cascade of events leads to the release of adenosine and the of vasoactive agents (Ko et al., 1990). Moreover, functional hyperemia is also mediated by glutamate-mediated Ca^{2+} waves in the astrocytes (Zonta et al., 2003). Additionally, there is evidence that direct and extensive neuronal innervation of smooth muscle cells can also control blood flow (Hamel, 2004; Mulligan and MacVicar, 2004), and astrocytes can increase CBF by releasing K+ ions from their endfeet onto arterioles. The astrocytes belong to a group of perivascular cells, or pericytes, that possess contractile properties that engage in the fine-scale control and maintenance of arteriolar and capillary tone (Bergers and Song, 2005).

Pericytes play a crucial role in the formation and functionality of the selectively permeable space that is the blood-brain barrier. The BBB is unique to the central nervous system, and regulates the delivery of important nutrients to the brain through active and passive transport mechanisms and prevents toxins from entering the brain (Zlokovic, 2008). Conversely, BBB disruption is a classic marker of vascular dysfunction.

Functional imaging of brain physiology

Functional MRI methods do not image neuronal activity directly; instead, they target the detection of changes in its various physiological correlates. When fMRI is mentioned, the blood-oxygenation level-dependent (BOLD) technique almost always comes to mind. First demonstrated by Ogawa et al. (1990), BOLD imaging relies on the paramagnetic properties of deoxyhemoglobin (dHb) in blood (Thulborn et al., 1981) and on intact neurovascular coupling. That is, the increase in cerebral oxidative metabolism ($CMRO_2$) that follows a surge of neuronal activity is normally associated with an enhanced cerebral blood flow (CBF) and blood volume (CBV) to the activated area, introduced earlier as functional hyperemia. The converse appears to take place during decreases in neuronal activity. Such changes are consistent with the classic view of neuronal energetics, and result in changes in the intravascular content of dHb, with increasing dHb content leading to MR image intensity reduction.

The superior sensitivity and relative technical simplicity of BOLD imaging have resulted in its unequivocal dominance in the field of fMRI. However, fMRI is not confined to BOLD imaging. Rather, fMRI encompasses a family of non-invasive imaging techniques that provide information on multiple aspects of brain function and physiology. Perfusion-based fMRI techniques target CBF and CBV in both the static and dynamic sense. With minor modifications, perfusion fMRI methods can also provide estimates of the arterial-transit time (ATT), which further describes cerebral hemodynamics (Wang et al., 2013). Moreover, a combination of blood-oxygenation and blood flow measurements enables the estimation the oxygen-extraction fraction (OEF) and $CMRO_2$ (Hoge, 2012). While most existing fMRI methods do not require exogenous contrast injections, contrast agents can also allow for the mapping of blood-brain barrier (BBB) permeability (Barbier et al., 2002), a key indicator of vascular health. In this review, we will not delve into molecular fMRI methods (Bartelle et al., 2016) that directly target metabolites and neurotransmitters, which are nonetheless integral to maintaining brain function. Also, the various fMRI techniques are described in more detail in this section in the context of the measures that they provide. In an endeavour to provide sufficient breadth and context, the techniques are further categorized as “established” and “emerging”, as their adoptions in clinical research are vastly different.

Established methods

The relatively established fMRI methods mainly target the measurement of vascular health, entailing the mapping of perfusion and cerebrovascular reactivity. Having been proposed more than 20 years ago, these techniques have generally been validated for sensitivity, specificity and reproducibility, with very encouraging translational track records. However, data interpretation should always be done in considering the assumptions involved in each technique.

Contrast-enhanced perfusion imaging

The first application of MRI in perfusion imaging (the imaging of CBF and CBV) relied on the injection of contrast agents. Dynamic susceptibility-contrast perfusion imaging (DSC MRI) capitalizes on the contrast-agent induced dynamic changes in the transverse relaxation (T2 or T2*) of blood and brain tissue to derive quantitative CBF and CBV as well as tissue mean-transit time (Barker et al., 2013; Ostergaard et al., 1996). Mostly commonly used as a blood-pool contrast agent in human studies is gadolinium-DTPA. DSC perfusion was rigorously validated against positron-emission tomography (PET) (Grandin et al., 2005; Sakoh et al., 2000), single-photon emission computed tomography (SPECT) (Wirestam et al., 2000) as well as X-ray computed tomography (CT) (Wintermark et al., 2005), and has well-established application in cerebrovascular diseases (Barker et al., 2013). However, the accurate identification of an arterial input function in the presence of possible occlusions has been a continual challenge (Chen et al., 2005; Yin et al., 2014) use of DSC MRI in measuring functional physiology has been less common (Frahm et al., 2008), as the rapid contrast washout would necessitate continuous infusion of contrast agents, limiting the feasibility of such techniques in providing dynamic CBF and CBV information. Furthermore, compromised BBB results in a loss of intravascular susceptibility contrast and severe perfusion-measurement inaccuracies (Sourbron et al., 2009).

Perfusion imaging

The predominant perfusion fMRI methods are based on endogenous contrast generated through blood water (Kwong et al., 1995), and was used in the first CBF-based fMRI experiment (Belliveau et al., 1991). Notably, arterial-spin labeling (ASL) (Detre et al., 1992) techniques rely on contrast generated by a magnetic label applied to inflowing arterial blood. After a certain post-labeling delay, as the tagged blood flows into tissue and exchange water with local tissue in a manner that is dependent on the flow rate. By fitting the difference between the tag and control (without tag) signals to a tissue-blood water exchange model (Buxton et al., 1998), quantitative CBF can be estimated. Moreover, dynamic changes in CBF in response to vascular stimuli or functional tasks can be derived from the time-series ASL images without the quantification step (Buxton et al., 1998; Wong et al., 1997). ASL perfusion measurements have also been validated repeatedly against those of PET (Chen et al., 2008; Ye et al., 2000).

While the first instance of ASL involved the use of a continuous radio-frequency (RF) irradiation to generate the magnetic label (hence its is termed continuous ASL, CASL) (Detre et al., 1992), impediments in the forms of extra hardware requirements and enhanced magnetization-transfer effects lead to the development of pulsed ASL (PASL) techniques (Barbier et al., 2001; Detre et al., 1992). PASL methods dominated a decade of fMRI studies (Wong et al., 1999) and have found their way into routine clinical studies (Telischak et al., 2014; Théberge, 2008; Wierenga et al., 2014). Moreover, by acquiring data at two different echo times (“dual echo”), CBF and BOLD contrast can both be extracted from ASL data. However, the brief RF label used in PASL leads to low CBF-contrast in cases of prolonged post-labeling delays (e.g. for patients) as well as high CBF estimation variability in the presence of heterogeneous regional arterial-arrival times. Efforts to overcome these challenges gave birth to pseudo-continuous ASL (pCASL) (Dai et al., 2008). The magnetic label in pCASL is performed through a train of pulsed RF labels, allowing for longer magnetic labels as well as longer post-labeling wait times but without the need for specialized hardware. It should be noted that the labeling efficiency of the pCASL pulse train can fluctuate with flow velocity, flow orientation and magnetic-field homogeneity, and solutions have been proposed to account for these caveats (Aslan et al., 2010; Han et al., 2016; Jung et al., 2012). At the time of this

review, the superior perfusion contrast offered by pCASL has propelled it into the de facto standard in ASL fMRI (Teeuwisse et al., 2014).

Cerebrovascular reactivity mapping

Cerebrovascular reactivity (CVR) is a well-established indicator of vascular reserve and autoregulatory efficiency. CVR decline has been associated with normal aging, and is the most reliable neuroimaging predictor of impending cerebrovascular disease (Pillai and Mikulis, 2015). Monitoring CVR in the elderly can provide critical therapeutic and scientific insight.

Qualitative CVR information can be gleaned from the fMRI response to any task (Dumas et al., 2012), but when quantitative CVR values are desired, vascular agents are generally required. Vascular agents used for CVR measurement generally include acetazolamide injection and CO_2. The latter is reflected in changes in $PETCO_2$, a surrogate for arterial CO_2 ($PaCO_2$) (Battisti-Charbonney et al., 2011). The role of CO_2 as a potent vasodilator has been described earlier. CBF increases by 3–4% per mmHg increase of $PETCO_2$, reaching its highest level when $PETCO_2$ is elevated by 10–20 mmHg above normal resting value (Brugniaux et al., 2007). CVR is normally symmetric across hemispheres and homogeneously distributed in grey matter (van der Zande et al., 2005). While fMRI is not the most established method of assessing CVR, it offers marked advantages over older methods, including richer spatial information and reduced invasiveness (Iannetti and Wise, 2007). Thus, CO_2-based CVR measured using fMRI has been widely applied to studying brain health, and has been extensively cross-validated (Herzig et al., 2008). Typically, CVR is measured as the ratio between changes in the BOLD signal and in $PETCO_2$, but can equally be measured using the CBF signal (Halani et al., 2015).

Robust $PETCO_2$ elevation (hypercapnia) can be induced through manually adjusted administration of blended gases (Cohen et al., 2004), end-tidal forcing (Poulin et al., 1996) or more recently, computerized $PETCO_2$ targeting (Mark et al., 2010; Slessarev et al., 2007). The latter method also provides immediate and robust $PETCO_2$ suppression (hypocapnia) (Blockley et al., 2011), and has been proposed as part of a rapid CVR-mapping protocol (Blockley et al., 2017, 2011).

CO_2-based CVR quantification was previously implemented mainly using transcranial Doppler ultrasound (TCD) (Ainslie and Duffin, 2009), PET (Ito et al., 2001) and dynamic computed CT (Chen et al., 2006). More recently using fMRI, CVR has been reliably assessed in both grey and white matter (Thomas et al., 2014). In the absence of a CO_2 delivery apparatus, breathing challenges including breath-holding and cued deep breathing (Bright et al., 2009) have been proposed as alternative ways to modulate $PETCO_2$. A comparison of breath-holding and inhaled-CO_2 approaches reveals important CVR dependence on methodology (Tancredi and Hoge, 2013). Furthermore, the reproducibility of both approaches have been established in healthy young controls (Bright and Murphy, 2013; Kassner et al., 2010).

Very recently, resting-state methods that do not require CO_2 perturbation have also been proposed (Golestani et al., 2016; Jahanian et al., 2017; Liu et al., 2017). Resting-state CVR methods rely on intrinsic fluctuations in the BOLD fMRI signal, and may significantly broaden the accessibility of CVR mapping to clinical researchers. Additionally, beyond the magnitude of CVR, the dynamic features of the fMRI response can also provide useful information. A slowing of the CVR response has been shown to characterize vascular lesions (Poublanc et al., 2015), adding a dimension to the utility of CVR mapping.

CVR mapping will be covered in a comprehensive review in this special issue, and will not be detailed here. However, it is critical to note that while CVR is defined as a blood-flow response (as is the case in TCD, PET and CT), the BOLD signal is modulated by both CBF and CBV as well as baseline oxidative metabolism, not to mention a series of field-dependent physical variables. Thus, the assumption of a linear relationship between the BOLD and CBF responses to CO_2 may at times be tenuous. Specifically, it is widely known that the BOLD response varies with CBF in a non-linear fashion (Hoge et al., 1999). This nonlinearity is superimposed in the vasculature's own nonlinear response behaviour to CO_2 (Battisti-Charbonney et al., 2011). Such nonlinear CVR changes have been demonstrated through a comparison with CBF-based CVR measurements at various vascular baselines (Halani et al., 2015), and may in a small part underlie the BOLD response behaviour in the "vascular steal" phenomenon (Sobczyk et al., 2014). This limitation will require careful consideration in the presence of known vascular dysfunction (Battisti-Charbonney et al., 2011).

Emerging methods

The emerging methods are less used in the clinical arena, but their importance cannot be overstated. It is understood that some of these techniques will require less translational effort than others and that not all of these techniques will find clinical uptake, but being made aware of them and working towards accelerating their translation should be a main target for neuroimaging researchers in the coming decade.

Arterial-transit time

By acquiring ASL images at multiple postlabeling delays (i.e. multi-delay ASL), the arterial-transit time (ATT) can be estimated as the delay time associated with the maximum control-tag signal difference (Poublanc et al., 2013; Qiu et al., 2010; Wang et al., 2003, 2014). The ATT is an indicator of cerebral hemodynamics, being prolonged in older subjects as well as patients suffering from cerebrovascular disorders (Detre and Alsop, 1999; Wang et al., 2014). Multi-delay ASL can be used with either PASL or pCASL labeling schemes to allow for more accurate characterization of CBF (Parkes, 2005).

Contrast-free mapping of cerebral-blood volume

Thought related to CBF, CBV offers unique diagnostic information (Siegal et al., 1997), and dynamic CBV is particular useful for isolating vascular from metabolic contributions to the BOLD fMRI signal (Hoge, 2012). The well-known power-law relationship first reported by Grubb et al. (1974) only relates CBF and CBV in their static than dynamic states. To date, three approaches to non-invasive dynamic CBV monitoring for fMRI have been introduced. The first, introduced by Lu et al. attempts to isolate blood from tissue based on blood-tissue longitudinal relaxation differences and has been termed vascular space occupancy (VASO) (Lu et al., 2003). This method has since been extended for mapping quantitative CBV (Hua et al., 2011). Other methods, including MOTIVE (Kim and Kim, 2005) and VERVE (Stefanovic and Pike, 2005), sought to isolate arterial and venous CBV changes, respectively. CBV-mapping techniques are extensively described in a recent review (Hua et al., 2018), and will not be repeated here. It should be mentioned, however, that an important consideration for both CBV and CBF mapping using fMRI methods is the role of blood-brain barrier permeability (Wu et al., 2010).

Despite the diagnostic utility of CBV measurements, the adoption of CBV techniques has been modest (Donahue et al., 2009), with VASO leading clinical translation. Though non-invasive, techniques such as VASO and MOTIVE rely upon a number of assumptions regarding blood and tissue properties, while VERVE carries high power deposition, heavy modeling requirements and limited spatial coverage. Without a feasible way to isolate arterial and venous CBV quantitatively, most CBV studies are limited to quantifying total CBV, as is provided by contrast-enhanced or VASO CBV techniques.

Blood-brain barrier permeability

Quantitative measurement of BBB permeability (Tofts and Kermode, 1991) has been performed based on dynamic contrast-enhanced (DCE) MRI (Barbier et al., 2002; Li et al., 2016; Wu et al., 2010), commonly using gadolinium. In brief, in the presence of BBB disruptions, the accumulation of contrast material in the extravascular extracellular space (EES) of affected tissues leads to increased T_1 relaxation and, therefore, increased signal intensity in T_1-weighted images. However, customized DCE MRI can also be used to provide perfusion contrast (Li et al., 2000).

Quantitative BBB permeability is computed by modeling contrast exchange between blood and the EES. For a detailed description of the methodology, we will defer to a recent review on the topic (Heye et al., 2014). The main caveats of permeability measurement include attention to contrast dosage and the influence of typical scanner instabilities.

The oxygen-extraction fraction (OEF) is the ratio between the rate of cerebral O_2 metabolism and delivery. The link between OEF and oxidative metabolism ($CMRO_2$) as well as CBF is illustrated in Fig. 2. The conventional standard method for mapping OEF and $CMRO_2$ has been ^{15}O PET (Fox and Raichle, 1986), but in the context of broader adoption, PET is disadvantaged by its lower spatial resolution, lower signal-to-noise and higher invasiveness.

Global OEF has been estimated using fMRI methods based on in vivo MR relaxometry of venous blood (Chen and Pike, 2010; Lu et al., 2012; Qin et al., 2010) and on the phase of deoxygenated blood (Jain et al., 2012). Notably, the T_2-relaxation-under-spin-tagging (TRUST) method (Lu et al., 2012), which estimates venous oxygenation (and hence OEF) using the known relationship between blood T_2 and oxygenation, has been validated using pulse oximetry. Furthermore, based on the Kety-Schmidt principle, OEF estimates have been converted to estimates of global $CMRO_2$ with the help of phase-contrast based arterial flow measurements (Chen and Pike, 2010). The Kety-Schmidt based methods do not provide spatially resolved measurements, and are hence not "imaging methods" per se (i.e. the focus of this review). Furthermore, the accuracy of T_2-based techniques such as these relies on accurate knowledge about the oxygenation dependence of T_2 at any given field strength. The TRUST method further relies the isolation of venous blood from other tissue types through flow labeling of descending flow, failures in which would result in OEF underestimation.

In terms of regional-specific $CMRO_2$ mapping, a wealth of research has centred around calibrated BOLD fMRI (Davis et al., 1998; Hoge et al., 1999). The calibrated-BOLD model assumes, among many things, that (1) both positive and negative vascular responses are a result changes in oxygen metabolism; (2) the relationship between changes in CMRO and CBF is largely fixed during a task block; (3) the intravascular BOLD signal contribution is negligible. In using calibrated fMRI to map brain activity, anaerobic metabolism is largely ignored. The first instance of calibrated fMRI called for the use of hypercapnia, which presumably induces a purely vascular response (without $CMRO_2$ involvement) that is required in parameterizing the quantitative BOLD model. Hypercapnia can be induced through inhaled CO_2 or breath-holding, similar to the case of

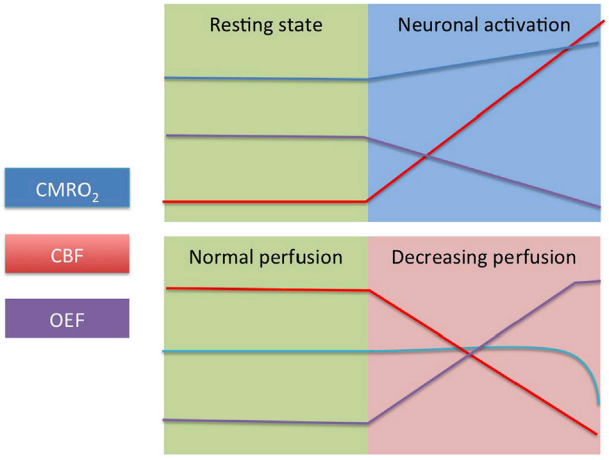

Fig. 2. Interactions amongst $CMRO_2$, CBF and OEF. All three remain relatively stable during normal brain function (shaded green). During neuronal activation (shaded blue), the increase in CBF overcompensates the increase in CMRO2, resulting in an overall decrease in OEF which gives rise to a higher BOLD signal. During vascular dysfunction (shaded pink), perfusion can consistently decrease, forcing OEF to rise in order to maintain $CMRO_2$.

CVR measurement. An alternative calibration approach is through hyperoxia, assuming that O_2 modulation does not induce vascular changes (Chiarelli et al., 2007a). However, both sets of assumptions may not hold under all circumstances. Thus, both hypercapnia and hyperoxia have been included in a comprehensive calibration model (Gauthier and Hoge, 2012), with the advantage of relaxing the assumptions of both earlier models, but strict subject cooperation is still required. The promise of gas-free calibration has also been proposed, based on the estimation of baseline tissue oxygenation via T_2 and T_2* (Blockley et al., 2015; Lu et al., 2011a). That is, T_2' is proportional to $CMRO_2$ divided by CBF × CBV. The major limitation, however, is that a calibration factor that relates the T_2* (hence T_2') value to the M value needs to be estimated, and this calibration factor is sequence dependent. One of the alternatives to calibrated fMRI is a technique termed quantitative BOLD, or "qBOLD" (He et al., 2008), which has been proposed for OEF estimation based on the interplay between T_2 and T_2* decay. The main challenges in broadening qBOLD's application is the need to fit sometimes-noisy data to a multi-parametric model. Another novel approach, "quantitative imaging of extraction of oxygen and tissue consumption (QUIXOTIC) (Bolar et al., 2011), uses venular-targeted velocity-selective spin labeling to isolate venous blood, followed by rapid refocusing to induce T_2 sensitivity in the venous signal. The T_2 is in turn related to venous oxygenation (like in the TRUST method), which, in combination with CBF measurements, can be used to derive voxel-wise quantitative $CMRO_2$. The main drawbacks of QUIXOTIC include the need to select a cutoff flow velocity for targeting venular blood flow as well as the long scan time, which the recently proposed turbo QUIXOTIC method attempts to remedy (Stout et al., 2018).

Yet another alternative to calibrated fMRI is susceptibility-weighted imaging (SWI). The phase images generated by SWI can be used to estimate OEF changes in response to stimuli or challenges (Zaitsu et al., 2011). Quantitative susceptibility mapping (QSM), which does not require gas challenges, is based on the linear dependence of magnetic susceptibility on dHb concentration (Spees et al., 2001). QSM has been used to quantify blood oxygenation in veins (Fan et al., 2012; Haacke et al., 1997) and brain tissues (Zhang et al., 2016). More specifically, maps of task-induced $CMRO_2$ and OEF changes can be computed using QSM and ASL data (Zhang et al., 2014). The main challenges facing QSM include the need to solve an ill-posed inverse problem as well as the dependence of QSM estimates on slice orientation. To provide perspective, QUIXOTIC shares similar limitations with TRUST, while QSM is still contingent on an accurate knowledge of venous orientation. Both of these methods are also currently limited by their lengthy scan times, while the qBOLD model is still under development. Efforts to streamline methods such as calibrated BOLD will likely bring about promising growth in clinical translation. Moreover, the superior versatility of fMRI allows numerous alternatives in multimodal integration, such as with near-infrared spectroscopy (NIRS) in the study of aging (Agbangla et al., 2017).

Neurovascular coupling

Although the neurovascular coupling (NVC) ratio classically relates CBF and $CMRO_2$, it is possible to extract such information without quantifying the $CMRO_2$ response, by measuring the BOLD and CBF task responses simultaneously; a similar neurovascular correlate was applied to resting-state fMRI data (Tak et al., 2014). Such an approach bypasses the confound of age-dependence on task performance and can reveal intrinsic traits of the NVU. Specifically, given the same level of BOLD response, a higher CBF response in older than young adults (Ances et al., 2009) suggests an altered NVC ratio. This could be explained by either (1) a higher $CMRO_2$ increase in response to task requirements, or (2) a hypoperfused baseline, a common finding amongst aging clinical populations (see Table 1). The fractional nature of relative BOLD and CBF measurements leads to such ambiguities, making interpretation critically dependent on additional quantitative metrics, such as baseline CBF and baseline blood oxygenation.

Table 1
Physiological fMRI of normal aging: selected human studies.

Reference	Cohort and Technique	Findings
(Bangen et al., 2009)	15 young and 15 older healthy controls; BOLD and CBF data measured using dual-echo PASL at 3 T	Older adults had significantly lower medial-temporal resting state as well as significantly higher CBF response to picture-encoding task (but not BOLD response) compared to young adults. These differences are associated with stroke risk.
(Restom et al., 2007)	15 young and 12 older healthy controls; BOLD and CBF data measured using dual-echo PASL at 3 T	Compared to young adults, older adults had significantly lower resting CBF in the medial-temporal region, as well as a higher fractional CBF response to picture encoding, but not a higher BOLD response.
(Thomas et al., 2014)	15 young and 15 older healthy controls; CVR measured using BOLD response to CO_2 inhalation at 3 T	White matter CVR response is higher and faster in the older controls, in contrast with grey matter.
(Chen et al., 2011)	11 young, 38 middle-aged and 37 older healthy controls (aged 22–88 years); CBF measured using PASL at 3 T	CBF declined with advancing age in the superior-frontal, orbito-frontal, superior-parietal, middle-inferior temporal, insular, precuneus, supramarginal, lateral-occipital and cingulate regions. Subcortical grey-matter CBF was preserved.
(Xekardaki et al., 2015)	75 cognitively healthy older controls, 73 controls with cognitive complaints and 65 MCI; CBF measured using PASL at 3 T	CBF in the posterior cingulate was statistically highest in the cognitively healthy group and lowest in MCI.
(Lu et al., 2011b)	232 healthy controls (aged 20–89 years); CBF measured using phase-contrast MRI, CVR measured using BOLD fMRI during CO_2 inhalation; OEF and $CMRO_2$ measured with help from the TRUST method, all at 3 T	$CMRO_2$ increased significantly with age, while CBF and CVR decreased with age.
(Gauthier and Hoge, 2012)	31 young and 31 older healthy controls; CVR measured using dual-echo pCASL at 3 T	Older adults have lower BOLD and CBF CVR, and a lower maximum-achievable BOLD signal (M value) than young adults.
(Montagne et al., 2015)	24 healthy adults aged 20–90 years; BBB permeability measured using DCE MRI	BBB permeability increased with age in the hippocampus.

Fmri in studying aging and neurodegeneration

Aging-related brain-physiology changes have traditionally been studied using MR spectroscopy (MRS), EEG (correlates of $CMRO_2$) (Dekoninck et al., 1982), TCD (CBF and CVR) (Peisker et al., 2010), PET ($CMRO_2$ and OEF, see review by (Newberg and Alavi, 2010)), SPECT (CBF) (Dormehl et al., 1999) and CT (CBF and CBV) (Meyer et al., 1994), and more recently using NIRS (Schroeter et al., 2004). A summary of conventional imaging tools can be found in a previous review (Gupta et al., 2012). Compared to these techniques, fMRI-based methods are advantageous in terms of reduced invasiveness (compared to PET, SPECT and CT), enhanced spatial coverage and detail (compared to TCD and NIRS) and uniqueness of contrast (compared to all other methods). These important advantages have led to more widespread acquisition of physiological fMRI in aging (Lu et al., 2011b). However, as will be demonstrated in subsequ (Chiarelli et al., 2007b)ent sections, the vast majority of studies in aging and neurodegeneration summarized in this review are based on the more established methods, namely ASL, DSC MRI and CVR. The uptake of novel fMRI methods for mapping brain physiology is still quite low. While to be expected, this delay in technical translation has resulted in a heavy bias in current fMRI literature towards vascular measures, which only provide a partial view of the neurodegeneration phenomenon.

As described earlier, in the presence of age-related vascular and metabolic changes, fMRI methods may be biased by the very changes that they aim to uncover, cautioning the interpretation of fMRI-based results in the context of dysfunction. This is true of established as well as novel methods.

Physiology of brain aging

The process of "normal aging" depends on genetic and environmental factors, and can vary widely across individuals. Nonetheless, the study of age effects in the living brain has mostly been based on comparisons amongst age groups. Within this context, decades of neuroscience research have led to consensus regarding certain functional aspects of normal (or healthy) brain aging (Yankner et al., 2008): (1) memory loss on several fronts, including delayed verbal memory recall, reduced working memory recall as well as long-term memory decline; (2) compromised executive function; (3) behavioural alterations, perhaps as a result of the former two changes. In the normal aging brain, reduced neural activity was found to first occur in the subiculum and the dentate gyrus instead of the hippocampus (Small et al., 2002). Conversely, reduced hippocampal activation has been observed in healthy aged adults during memory-related tasks (Rémy et al., 2004).

Underlying the various functional phenotypes of aging, histopathological, electrophysiological and nuclear-imaging studies have revealed accumulating oxidative stress, declining mitochondrial function and reduced cellular regeneration (Rossini et al., 2007). The elevated intracellular Ca^{2+} concentrations in older adults main sustain normal neuronal functional only until this fragile state of Ca^{2+} homeostasis is disrupted by vascular dysfunction (Toescu and Verkhratsky, 2004). Indeed, advancing age is also the biggest risk factor for vascular diseases such as hypertension, diabetes and stroke, which are also the top risk factors for dementia (Girouard and Iadecola, 2006) As well, BBB breakdown has been known to occur as part of normal aging (Rosenberg, 2014), compromising the function of the NVU. As cerebrovascular efficiency falls, the aging brain may also suffer from impaired glucose metabolism, although this may be mediated by brain atrophy (Ibáñez et al., 2004). Indeed, cortical atrophy has been widely reported and robustly observed (Salat, 2004), particular in the paracentral cortex, the superior and inferior frontal gyri as well as the superior temporal gyrus (Fjell et al., 2009). Furthermore, age-related white-matter degeneration is related to cardiovascular risk (Artero et al., 2004) and reduced CBF and CVR (Chen et al., 2013; Marstrand et al., 2002; Thomas et al., 2014). These known physiological targets have lent themselves to the identification of fMRI-based physiological markers.

A summary of recent human literature can be found in Table 1. In accordance with the documented decline in cerebrovascular health, reduced CBF in older adults, both regionally and globally, has been widely observed (Chen et al., 2013, 2011; Lu et al., 2011b; Tarumi et al., 2014), while accounting for concurrent age effects in brain-volume. This has been associated with both increasing arterial stiffness (Heffernan et al., 2008) and cognitive decline (Xekardaki et al., 2015). Reports on CVR have been more limited, but fMRI-based CVR is found to decline with advancing age in both the grey and white matter (Lu et al., 2011b; Thomas et al., 2014), concurrent with observations of increased BBB permeability (Montagne et al., 2015). Moreover, a higher ΔCBF-ΔBOLD ratio in older adults in response to function tasks points to altered neurovascular coupling (Ances et al., 2009; Bangen et al., 2009; Restom et al., 2007), in that the ΔCBF-$CMRO_2$ ratio may decrease with advancing age. This is consistent with reduced CBF in aging, but does not preclude the existence of an exaggerated $CMRO_2$ response. This question was clarified through calibrated BOLD (Gauthier et al., 2012), which revealed that resting blood oxygenation is also lower in the elderly, and that the $CMRO_2$ contribution to any given BOLD response is likely to increase

with age. Conversely, in a separate study, the CBF and $CMRO_2$ responses to a simple sensory stimulus is found to be maintained in aging, suggestive of lower baseline blood oxygenation in older adults (Ances et al., 2009) Lastly, whole-brain resting $CMRO_2$ was reported to rise with age (Lu et al., 2011b), which may reflect reduced neuronal computational efficiency. However, this is in contradiction with previous PET-based findings (Baron and Marchal, 1992; Leenders et al., 1990) as well as with those using MRS (Boumezbeur et al., 2010), consistent with age-associated reductions in the concentration of the metabolite N-acetylaspartate (Schmitz et al., 2018).

While brain atrophy could have biased the PET measurements of CBF and $CMRO_2$, atrophy does not account for all discrepancies. Taken together, these findings may also be evidence that there are multiple streams/stages of brain aging. In the "optimistic" stream involving relatively healthy older adults, increased $CMRO_2$ is required to sustain normal brain function in the elderly, compensating for the decline in performance despite a decline in perfusion; when the compensation mechanism starts to fail, possibly due to underlying vascular risks in asymptomatic elders, then brain metabolism will conceivably decline also (Sperling et al., 2003). In this regard, the heterogeneity in cohort sizes and selection across aging studies has certainly contributed to discrepancies in the experimental findings, and caution in interpretation is warranted.

Furthermore, it is instructive to recall the assumptions and limitations associated with current fMRI methods, notably with respect to transit-delay-related CBF biases in ASL and CVR nonlinearity effects mentioned in earlier sections. For instance, when ASL is used, a post-labeling delay too short for the elderly will lead to CBF underestimation and hence $CMRO_2$ overestimation. These limitations also apply to the study of aging-related neurodegeneration, and call for the integration of multiple physiological measures.

Age is the biggest risk factor for neurodegenerative diseases. The prevalence of dementia increases almost exponentially with increasing age with around 20% of those aged 80 affected rising to 40% of those aged 90 (Lobo et al., 2000). The dementia types seen most frequently in the elderly are AD accounting for around 40%–70% of dementias, and vascular dementia (VaD) 15%–30% (Lobo et al., 2000).

Physiology of aging-related neurodegeneration

Aging-related neurodegeneration is a leading cause of disability and death amongst the aging populations worldwide, and there are currently no disease-modifying therapies (Brettschneider et al., 2015). Neurodegeneration generally refers to the slow and progressive dysfunction and loss of neurons and axons in the central nervous system (Amor et al., 2010). It has been suggested that chronic neurodegeneration in aging commonly results from misfolding of proteins (Jové et al., 2014). That is, the decline of antioxidant defense and repair mechanisms have been associated with accumulating oxidative damage that lead to neurodegenerative disorders. While the root causes leading up to such damage are not fully understood, a general consensus has been reached in terms of the cerebrovascular contribution to cognitive impairment (Pluta et al., 2011).

Neurodegeneration is known to affect the constituents of the NVU and to alter neurovascular coupling. These alterations can include changes in both the neurochemical mediators of neurovascular coupling and the dynamics of the vascular system itself (D'Esposito et al., 2003; Iadecola, 2004). The vasculature is prone to its own deleterious processes brought about by main risk factors of neurodegeneration. Hypertension, as the chief risk factor, promotes vascular hypertrophy and atherosclerosis that leads to hypoperfusion (Girouard and Iadecola, 2006). Eventually vasculature would become increasingly torturous and less reactive, exacerbating cellular oxidative stress (Black et al., 2009). The compromised capacity for vasodilation or constriction is likely behind the observed disruptions in the relationship between vascular and neural responses.

To this day, disease diagnosis has largely been driven by clinically classifiable declines in cognitive function, although PET imaging of glucose metabolism provides higher diagnostic accuracy in the case of dementia, validated through autopsy (Jagust et al., 2007). Moreover, as shown in Fig. 3, structural brain changes may well precede clinical function changes. Structural imaging and histopathology can uncover changes in brain structure and cellular processes associated with disease (Brettschneider et al., 2015; Dugger and Dickson, 2017). However, in terms of interrogating the underlying pathophysiology in the living brain, which may show changes even earlier than structural changes, most of what is known has been learned through electrophysiological measurements (mainly using electroencephalography and magnetoencephalography) (Rossini et al., 2007). In relation to electrophysiology, the unique contribution of fMRI is its ability to provide access to vascular physiology, and in relation, the underlying metabolic process. These will be discussed in relation to specific diseases.

Cerebral amyloid angiopathy

Cerebral amyloid angiopathy (CAA) is caused by aggregated forms of extracellular neurotoxic beta amyloid (Aβ) that settle within vessel walls of small to medium arteries, including leptomeningeal and penetrating arteries (Roher et al., 1993). Evidence of Aβ entrapment in perivascular drainage has been widely found in CAA (Herzig et al., 2006) CAA is known to lead to impaired vascular reactivity and reduced perfusion (Miao et al., 2005; Weller et al., 1998). CAA is also associated with ischemic lesions and vascular cognitive impairment (Pluta et al., 2011), and could be a precursor to Alzheimer's disease (AD).

The majority of MRI studies involving CAA have been associated with the imaging of structural markers, such as microbleeds (Charidimou et al., 2017), cortical atrophy and white-matter lesions (Reijmer et al., 2017). Only recently has BOLD fMRI been used to assess CVR in CAA patients, reporting reduced CVR amplitude as well as response speed (Dumas et al., 2012; Williams et al., 2017). The recent literature is summarized in Table 2. These signs of compromise vascular function are consistent with observations Aβ accumulation in the tunica media, smooth muscle cells and adventitia (Pezzini et al., 2009), and are present in 95% of AD patients.

Dementia

Alzheimer's disease and mild cognitive impairment. Clinical AD is associated commonly with memory loss and loss of other cognitive functions, eventually premature death. As the most common cause of dementia, AD accounts for 60–80% of dementia cases (Lobo et al., 2000). The primary risk factor for the disease is aging. The disease is found in 2%–3% of individuals at the age of 65 years, growing to 25%–50% of the population above the age of 85 years (Gorelick, 2004). MCI is commonly considered an early or preclinical form of AD. However MCI is a heterogeneous condition, and the main phenotype that is associated with AD is amnesic MCI (aMCI).

Histological studies have relied primarily on immunocytochemical techniques to detect the presence of plasma or serum amyloid in the brain, and evidence supports that both inflammation and oxidative stress (increased level of ROS) occur early in AD (Erickson and Banks, 2013). Furthermore, AD has been associated with reduced metabolic activity and neuronal loss beginning in the entorhinal cortex and the CA1 region of the hippocampus (Gomez-Isla et al., 1996). As AD is only fully diagnosed on autopsy, AD patients are often classified as "probable AD". Although the precise causes of AD are unclear, the ε4 allele of the apolipoprotein E (APOE) is considered the main genetic risk factor, and is found in 40–80% of AD patients (Strittmatter et al., 1993) as well as all cases of early-onset AD (EOAD). In contrast, the closely related ε3 allele is considered neutral (Bertrand et al., 1995).

While the cholinergic hypothesis (Siegfried, 1993) proposes reduced synthesis of the neurotransmitter acetylcholine as the cause of AD, it has generally been believed in recent years that AD is induced by the

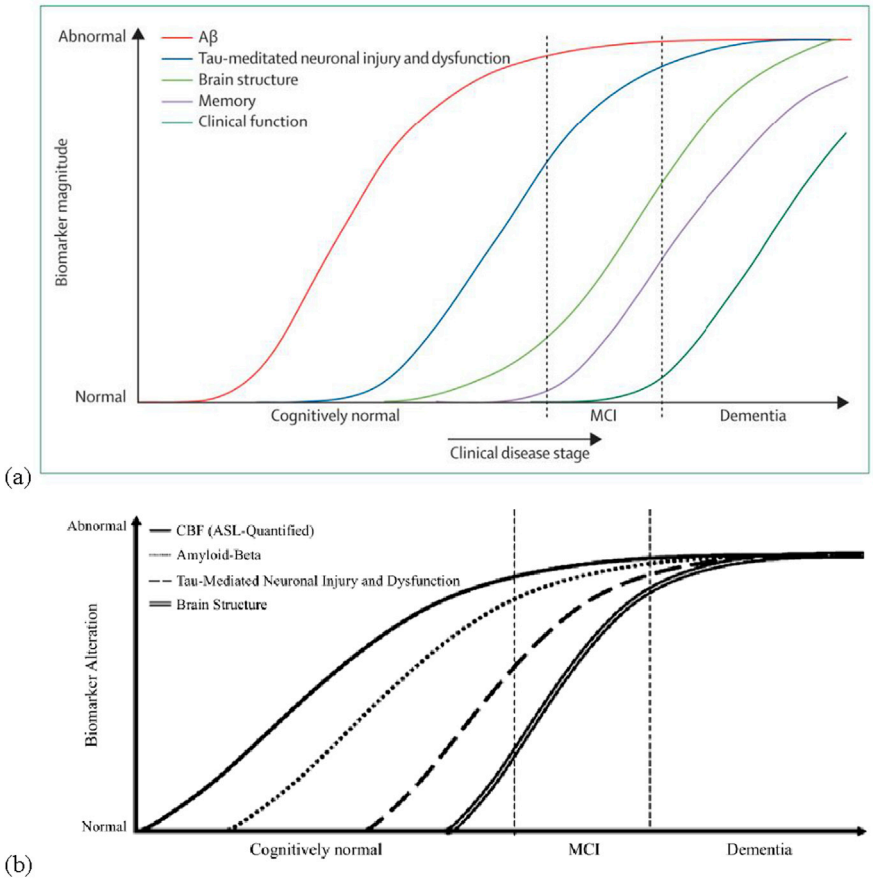

Fig. 3. Dynamic biomarkers of the Alzheimer's pathological cascade. (a) Aβ aggregation, which long precedes the display of structural changes (detected by anatomical MRI) and clinical symptoms, is likely to translate into detectable alterations in vascular health (figure taken from (Jack et al., 2010) with permission). (b) It is further suggested that CBF deficits can be present before Aβ accumulation is detected, making vascular markers an attractive target for disease prediction and prognosis. The figure is reproduced from (Wierenga et al., 2014) with permission.

Table 2
Physiological fMRI of in cerebral amyloid angiopathy: selected human studies.

Reference	Cohort and Technique	Findings
(Dumas et al., 2012)	15 CAA patients and 12 older controls; CVR measured using BOLD fMRI during visual task at 1.5 T	BOLD response (CVR) was reduced in amplitude and speed CAA group.
(Peca et al., 2013)	18 CAA patients and 18 older controls; neurovascular health measured using BOLD fMRI during visual and motor tasks at 3 T	Visual BOLD response was lower in patients, but not motor response. BOLD response reduction correlated with white-matter lesion volume and microbleed count.
(Williams et al., 2017)	13 CAA patients and 14 older controls; hemodynamic response (CVR) measured using BOLD fMRI during visual and motor tasks	The motor hemodynamic response was significantly lower, wider and slower in CAA. The response width correlated with microbleed count.

aggregation of extracellular Aβ, preceded by the formation tau neurofibrillary tangles that destroy the cellular cytoskeleton (Blennow et al., 2006). However, the animal literature reports that soluble Aβ, which predates Aβ plaques, deregulates cerebrovascular function by activating a free-radical cascade (Park et al., 2008). Indeed, 60–90% of AD patients exhibit cerebrovascular pathologies (Bell and Zlokovic, 2009). The vascular hypothesis of AD pathogenesis (de la Torre, 2010; de la Torre and Mussivand, 1993) is further supported by the predictive value CVR (Sato and Morishita, 2013) in terms of MCI-to-AD conversions (Buratti et al., 2015). Moreover, histological evidence points towards increased BBB permeability as a mechanism behind AD-related microvascular dysfunction (Brenner, 2008; Raz et al., 2016). Furthermore, it is increasingly recognized that vascular deficits may be the most accessible physiological treatment target in the effort to delay dementia onset, and approaches that enhance perfusion have demonstrated potential therapeutic value (de la Torre, 2016). Thus, fMRI-based physiological measurement are an appealing approach to shed light on potential early markers of AD progression and treatment.

The application of fMRI techniques to map CBF and CVR has flourished in the past decade and has made AD the most studied neurodegenerative disease using non-invasive fMRI methods. There have been comprehensive recent reviews on ASL-based perfusion mapping for imaging MCI and early AD (van Osch et al., 2011; Wang, 2014; Wierenga et al., 2014), which will not be repeated in this review. The current consensus, based on PET, SPECT and ASL studies, is that MCI and AD groups exhibit significantly lower CBF than age-matched controls, primarily observed in frontal and temporal cortical regions (Gao et al., 2013; Zou et al., 2014). CBF deficits are further shown to distinguish AD from other dementias (Binnewijzend et al., 2014). Specifically, both SPECT and PET-based measures of CBF deficits in the middle-temporal precuneus, posterior-cingulate and parietal association areas are found to be predictive of MCI conversion to AD (Hirao et al., 2005; Nobili et al., 2001). TCD-based CVR measurements have long been used to assess vascular-disease risk and severity (Maeda et al., 1993; Vicenzini et al., 2007), and the use of CO_2-based CVR mapping in AD has been reviewed recently (Glodzik et al., 2013), demonstrating the feasibility of using PET, SPECT, TCD and fMRI to detect reduced CVR in preclinical and clinical AD. CVR deficits have even been discovered amongst young APOE ε4 gene carriers (Hajjar et al., 2015; Suri et al., 2014) (Fig. 4). Such reductions in CVR echo postmortem observations of vascular dysfunction (Chow et al., 2007), and are the result of a number of structural changes in the vasculature, including CAA, astrocytic end-feet swelling, pericyte degeneration, basement-membrane hypertrophy and endothelial-cell metabolic abnormalities (Hashimura et al., 1991; Miyakawa et al.,

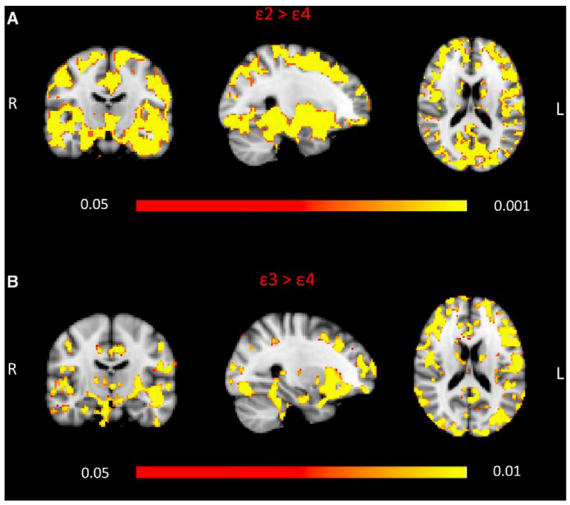

Fig. 4. The effect of ε4-carrier status on CVR amongst young adults. CVR is measured using mixed-air hypercapnia during BOLD fMRI scanning. Both (A) ε2-and (B) ε3-homozygotes have higher CVR relative to ε4-carriers. Red-to-yellow colors define voxelwise significance corrected for multiple comparisons. The figure is modified from (Suri et al., 2014) with permission.

1997). In the current review, we will provide a more general depiction of the state-of-the-art involving multiple physiological metrics, particularly in view of emerging fMRI methods that provide metabolic measures (Lajoie et al., 2017) (Fig. 5). Select human studies associated with these findings are summarized in Table 3.

The ASL-based findings of CBF deficits in frontal, temporal and parietal regions are consistent with earlier findings based on PET (Alsop et al., 2000) and SPECT (Varma et al., 2002, 1999). In contrast, a CBF elevation in the medial temporal region detected using ASL has been used to discriminate between APOE ε4 carriers and non-carriers even amongst cognitively healthy individuals (Bangen et al., 2012; Wierenga et al., 2012)The compromised CVR is consistent with TCD-based findings in the middle-cerebral artery (Viticchi et al., 2012). In relation to this, AD-associated decline in PET-based measurements of glucose metabolism has been associated with an increase in BOLD-signal fluctuation amplitude in the white matter, which has been suggested as a measure of vascular pulsatility (Makedonov et al., 2016), as AD has been associated with increased TCD-based pulse-wave velocity (Zhong et al., 2014). Lastly, based on calibrated BOLD, resting $CMRO_2$ in AD patients is found to be depressed in the parietotemporal and precuneus regions (Lajoie et al., 2017), consistent with PET findings (Ishii et al., 1996). However, as calibrated BOLD combines BOLD and CBF data, it is particularly prone to susceptibility artifacts and arterial-transit delays in older participants, as noted by Lajoie and colleagues. Nonetheless, the trend of $CMRO_2$ reduction is consistent with those reported using TRUST MRI in MCI patients (Thomas et al., 2017) and with MRS-based findings of reduced glucose metabolism (Mullins et al., 2018).

Despite the presence of vascular deficits in the majority of AD patients (up to 95% (Glodzik et al., 2013)), autoregulation may not be compromised (as was found in AD transgenic mice) (Zazulia et al., 2010) it is still unclear whether CBF abnormalities precede those in those in $CMRO_2$ in all cases of probable AD. Moreover, given the overwhelming influence of vascular risk factors in AD progression, the lines between perfusion deficits in AD and other types of dementia can become blurred in later stages of the disease, as will be discussed in later sections. As a case in point, given the rampant occurrence of CAA amongst suspected AD patients, the vascular dysfunction can produce deleterious oxidative stress that can promote ischemia and accelerate AD progression (Bookheimer and Burggren, 2009; Girouard and Iadecola, 2006). To test such a hypothesis, establishing a sensitive imaging marker of cerebral metabolism is critical. Furthermore, it is unclear whether CBF or CVR is a better potential biomarker of AD severity. It is conceivable that a diseased vasculature may sustain a normal perfusion level but reveal an abnormal response to a stress test such as used in CVR mapping (Fierstra et al., 2013). As an increasingly amount of CVR data is generated using BOLD MRI, it is also important to note that microvascular CVR is more reflective of AD severity (Jellinger and Attems, 2006), while the BOLD fMRI is generally dominated by large-vessels.

Vascular dementia. Vascular dementia (VaD), also known as vascular cognitive disorder, reportedly constitutes 10% of cognitive-impairment cases (Jellinger, 2007) and 15%–30% of dementia cases (Lobo et al., 2000). VaD is characterized by multi-infarct encephalopathy, white-matter lesions and hippocampal sclerosis among others, and results in deficits in cognition, memory, behaviour and executive functioning (Jellinger, 2008, 2007). On the basis of the vascular hypothesis, VaD is caused by diminished CBF, leading to hypoxia and BBB permeability from prolonged vasculotoxic and neurotoxic effects that promote neurodegeneration and amyloid deposition (Bell et al., 2010). Risk

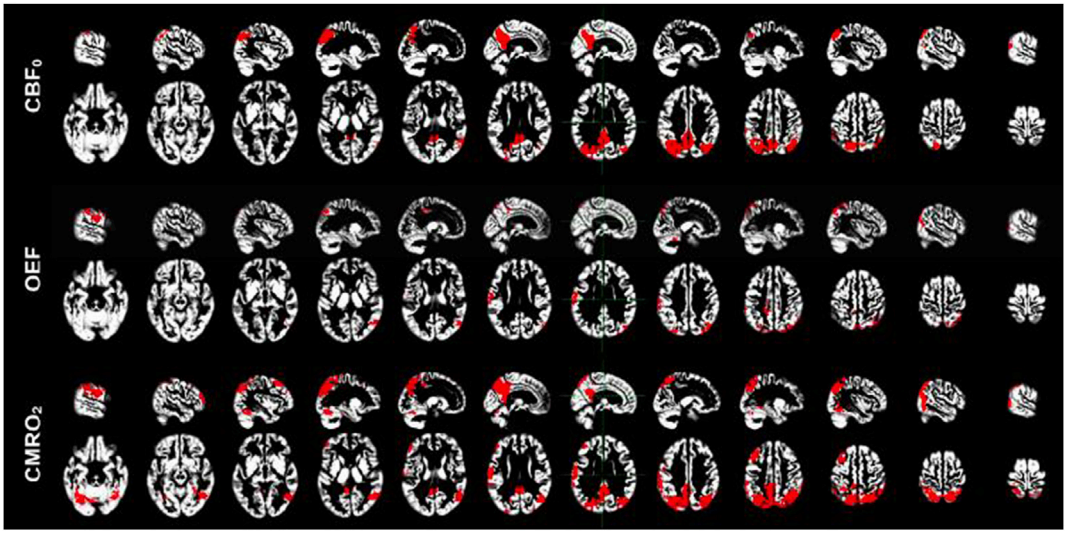

Fig. 5. Voxel-based analysis of AD-control differences in CBF, OEF and $CMRO_2$, adjusted for age. For each physiological variable, the coloured regions show a significant deficit in AD (family-wise cluster-corrected $p < 0.05$) CBF was measured using pCASL, whereas OEF and $CMRO_2$ are estimated using the comprehensive calibrated BOLD technique. $CMRO_2$ deficits are found to be more widespread than those in CBF and OEF. Figure is modified from (Lajoie et al., 2017) with permission.

Table 3
Functional MRI in physiological imaging of dementia and mild-cognitive impairment: selected human studies. In view of recent comprehensive studies on ASL-based perfusion imaging in MCI, AD, FTD, VaD and DLB, this summary aims instead to represent multiple aspects of physiology.

Reference	Cohort and Technique	Findings
(Wolk et al., 2011)	15 MCI and 25 healthy older controls; CBF measured using pCASL at 3 T	CBF in MCI is significantly increased in the medial temporal region (MTL).
(Bangen et al., 2012)	45 healthy older adults (29 APOE ε4 carriers and 15 non-carriers), 16 MCI (8 APOE ε4 carrier and 8 non-carriers); CBF mapped using PASL at 3 T	Healthy APOE ε4 allele demonstrated increased MTL resting state CBF relative to ε4 non-carriers, whereas individuals with MCI showed lower medial-temporal CBF than controls.
(Wierenga et al., 2012)	20 mild cognitive impairment (MCI; 11 ε3 and 9 ε4 carriers) and 40 healthy controls (27 ε3 and 13 ε4 carriers); CBF mapped using PASL at 3 T	Elevated resting CBF in parahippocampal and fusiform areas in healthy e4 carriers but decreased for MCI ε4 carriers. The opposite pattern was seen in frontal regions.
(Zou et al., 2014)	20 AD patients and 20 healthy older controls; CBF measured using PASL at 3 T	CBF in AD was significantly reduced in the bilateral frontal region, the temporal pole, the temporal-parietal junction and the hippocampus.
(Bron et al., 2014)	32 early-AD and 32 healthy older controls; CBF measured using PASL at 3 T	CBF was used to classify AD from controls with 86–91% accuracy.
(Gao et al., 2013)	26 AD and 23 VaD; CBF measured using PASL at 3 T, and CVR measured using CBF response during CO_2 inhalation.	For the AD group, CBF was significantly lower in both the bilateral frontal and temporal lobes in AD group. For the VaD group, CBF was lower in left frontal and temporal white matter. CVR calculated by CBF was impaired more severely in bilateral frontal cortices in AD.
(Tosun et al., 2016)	46 older controls (34 Aβ+, 12 Aβ-), 55 early MCI (30 Aβ+, 25 Aβ-), 20 AD (Aβ+); CBF measured using PASL at 3 T	Reduced CBF in posterior-inferior brain was best at discriminating Aβ+ from Aβ+ groups.
(Binnewijzend et al., 2014)	20 FTD patients, 14 DLB patients, 48 AD patients and 50 controls	In AD patients, CBF was decreased in all supratentorial regions, most prominently so in the posterior regions. DLB patients showed lowest CBF values throughout the brain, but temporal CBF was preserved. Supratentorial PVC cortical CBF values were lowest in the frontal lobes in FTD patients, and in the temporal lobes in AD patients.
(Roquet et al., 2016)	44 prodromal DLB, 16 mild DLB, 13 prodromal AD, 26 AD and 21 older healthy controls; CBF mapped using PASL at 3 T	DLB is associated with more CBF deficits in frontal, insular, and temporal cortices whereas AD showed reduced perfusion in parietal and parietotemporal cortices.
(Yezhuvath et al., 2012)	17 AD patients and 17 healthy older controls; CVR measured using BOLD fMRI scans during CO_2 inhalation, and CBF measured using pCASL	CVR in AD was significantly reduced in the prefrontal, anterior cingulate and insular regions, contrasting CBF reductions in the temporal and parietal regions.
(Asllani et al., 2008)	12 AD and 20 older controls; CBF measured using CASL at 1.5 T	CBF in AD was significantly reduced in the superior-temporal, cingulate, middle-temporal, fusiform, precuneus and inferior parietal regions.
(Verclytte et al., 2016)	37 patients with EOAD; CBF measured using pCASL	CBF was reduced in EOAD, with the most severe hypoperfusion located in the parietal lobes, the precuneus, the right posterior cingulate cortex, and the frontal lobes.
(Du et al., 2006)	21 FTD, 24 AD and 25 older controls; CBF measured using PASL at 3 T	CBF was reduced in the right frontal lobe in FTD patients, and higher CBF in FTD than in AD in parietal and posterior cingulate regions. CBF patterns correlate with judgment and problem-solving abilities, and improved classification accuracy of AD vs. FTD.
(Bron et al., 2014)	11 AD, 9 AD/FTD, 11 FTD and 32 older controls; CBF measured using pCASL at 3 T	CBF maps yielded successful patient classification but did not provide added accuracy to cortical-atrophy based classification.
(Schuff et al., 2009)	14 AD, 8 subcortical ischemic VaD, 18 older controls; CBF measured using PASL at 1.5 T	CBF was significant reduced in frontal and parietal cortices in AD and VaD, with CBF deficits additionally associated with white-matter lesions in VaD.
(Roquet et al., 2016)	46 prodromal DLB, 16 mild DLB, 13 prodromal AD, 25 mild AD and 21 older controls; CBF measured using PASL at 3 T	CBF in DLB was reduced relative to controls in frontal, insular and temporal cortices, whereas CBF in AD was reduced in parietal and parietotemporal regions.
(Steketee et al., 2016)	13 AD and 19 FTD patients, and 25 age-matched older and 22 younger controls; CBF measured using pCASL at 3 T	CBF was lower in the posterior cingulate in AD than in FTD. Compared to controls, AD patients had widespread CBF reduction whereas FTD patients showed CBF deficit mainly in anterior cingulate.
(van de Haar et al., 2016)	7 AD, 9 MCI and 17 older controls; BBB permeability measured using DSC MRI at 3 T	BBB permeability is significantly higher in AD and MCI groups compared to controls, in cortex, deep-grey matter and normal-appearing white matter.
(Starr et al., 2009)	15 AD and 15 older controls; BBB permeability measured using DCE MRI at 1.5 T	Mean BBB permeability was not different between AD and controls, but permeability-related signal increased more rapidly for AD group over time.
(Cantin et al., 2011)	9 AD, 7 MCI and 11 older controls; CVR measured using BOLD fMRI during CO_2 inhalation at 1.5 T	CVR was higher in control group, but not significantly different between AD and MCI groups; diffusion CVR deficits were observed but predominant in posterior brain areas.
(Richiardi et al., 2015)	15 aMCI, 20 AD and 28 older controls; BOLD fMRI during 7% CO_2 at 3 T	CVR correlated with cognitive decline, and is significantly lower in both the aMCI and AD groups.
(Suri et al., 2014)	18 APOE ε4-carriers, 17 APOE ε3-homozygotes and 18 APOE ε2-carriers, all under 40 years of age; CBF and BOLD fMRI measured using dual-echo pCASL; CVR was derived from BOLD signal during CO_2 inhalation	CVR was significantly higher in young adults carrying the APOE ε2 allele than in ε3 carriers, and the lowest are in ε4 carriers. No CBF differences was found between groups.
(Lajoie et al., 2017)	37 mild-moderate AD and 34 older controls; hypercapnia- hyperoxia calibrated fMRI using dual-echo pCASL at 3 T	CBF and $CMRO_2$ were reduced in the temporoparietal region. No frontal CBF reduction or global CVR reduction is found in the AD group.
(Thomas et al., 2017)	44 aMCI and 28 older controls; CBF measured using phase-contrast MRI, CVR measured using BOLD fMRI during CO_2 inhalation; OEF and $CMRO_2$ measured with help from the TRUST method, all at 3 T	Global CBF and CVR was not different between aMCI and controls, but $CMRO_2$ was significantly lower in aMCI.

factors for VaD include large-vessel disease, small-vessel disease and cardioembolic disease. In subcortical VaD, the neuropathology is driven by severe stenosis and microvessel occlusion, culminating as white matter ischemia and multiple lacunar infarcts in subcortical structures (Roh and Lee, 2014).

Compared to the case of AD, the use of physiological fMRI in VaD has been very limited. ASL has revealed that VaD is associated with a distinct spatial pattern of hypoperfusion compared to other dementias. The details can be found in Table 3. Specifically, ASL results revealed a VaD-specific hypoperfusion pattern in the temporal and frontal white matter, which is not observed in AD (Gao et al., 2013). However, the sensitivity of ASL to detect such distinguishing features in CBF is still uncertain (Schuff et al., 2009).

It has been postulated that classic VaD and AD models should be viewed as two disease extremes, one driven by hypoperfusion-induced ischemia and the other defined by Aβ-driven neurodegeneration. In practice, the two disease components often coexist. Moreover, VaD and AD share many risk factors and clinical manifestations (Gorelick, 2004; Iadecola, 2004), as well as hypoperfusion and reduced CVR, making their separation difficult in later stages of disease. More accurate identification of pathogenic processes requires disease monitoring in earlier stages as well as the ability to measure neurometabolic as well as vascular changes. In this regard, CBF alone is likely insufficient as a vascular measure, as it reflects both hemodynamic and neuronal modulation. A more vascular-centric measure such as CVR is likely more effective at detecting early vascular abnormalities.

Frontotemporal dementia. In contrast to AD, there is little evidence that frontotemporal dementia (FTD) is associated with cerebrovascular dysfunction. The role of tau neurofibrillary tangles in neurodegeneration is firmly established in frontotemporal dementia (Yankner et al., 2008), in which ~50% of patients report a positive family history, implicating genetic-driven pathogenesis (Rosso, 2003). There have been recent reports of tau pathology associated small-vessel disease (Thal et al., 2015). As these FTD-related observations are proposed to mainly reflect subcortical small-vessel disease, the application of fMRI techniques is more confined by the limited signal-to-noise properties of white matter (as compared to grey matter). Thus, there have been few fMRI-based brain-physiology studies involving FTD. ASL has been used to reveal differential patterns of hypoperfusion in FTD relative to AD (Steketee et al., 2016), as summarized in Table 3.

ASL perfusion reportedly distinguished FTD from AD with a 74% accuracy based on the FTD pattern of frontal hypoperfusion without concurrent parietal hypoperfusion, in line with earlier results based on SPECT (Archer et al., 2015; McNeill et al., 2006; Varma et al., 1999). With the appropriate technical advances and optimizations, the role of vascular impairment in FTD remains to be further investigated.

Dementia with Lewy Body. The term "Lewy-Body disease" refers to disorders characterized by the pathologic neuronal accumulations of intracellular vesicles and neurotoxic α-synuclein proteins known as Lewy bodies (Brettschneider et al., 2015; Pezzoli et al., 2017). In dementia with Lewy Body (DLB), the mitochondria are drawn into the Lewy body and hence mitochondrial integrity is lost. DLB is associated not only with cognitive deficits, but also motor dysfunction, sleep disorders and visual hallucinations (Pezzoli et al., 2017).

Some existing human fMRI studies on DLB are detailed in Table 3. The use of MRI in mapping DLB brain physiology is still in its infancy. Nonetheless, ASL fMRI has been successfully applied to DLB, revealing that, compared to AD and FTD, DLB is associated with the lowest overall CBF across the brain but relatively preserved temporal-lobe CBF (Binnewijzend et al., 2014). In a separate ASL study (Roquet et al., 2016), DLB is distinguished from AD through a lack of parietal hypoperfusion. These distinct hypoperfusion patterns are consistent with the differences in disease profiles, with DLB affecting mainly executive function and attention without inducing memory deficits. A general caveat of studying CBF in the frontal regions is the presence of strong susceptibility gradients in the medial orbitofrontal regions, which may compromise the sensitivity of CBF estimates.

Parkinson's disease

Parkinson's disease (PD) is the second most common neurodegenerative disorder after dementia (Van Den Eeden et al., 2003). As a primarily motor disorder that is characterized by tremours, bradykinesia or hypokeinesia, muscular rigidity and postural instability (Théberge, 2008), PD is also an age-related neurodegenerative disorder, with its prevalence increasing 20 fold to 4% amongst those over 80 years of age (Newman, 2009). The main clinical symptoms of PD are associated with the destruction or damage of dopaminergic neurons in the substantia nigra that are essential to the motor-control pathway. Though not yet clear, PD etiology has been associated with genetic factors, drug use and traumatic brain injury among others. Notably, the involvement of misfolded proteins (α-synuclein) that accumulate and form Lewy bodies (Whitworth and Whitworth, 2014) has linked PD to DLB as part of a disease spectrum. However, in PD, multiple Lewy bodies are often observed with a-synuclein interacting with genetic material to cause marked nuclear degradation (Power et al., 2016). Importantly, due to PD's comorbidity with DLB, as many as 40% of people who have PD will develop dementia, giving rise to the concept of PD dementia (Pezzoli et al., 2017).

The study of PD brain physiology using MRI has mainly been focused on perfusion imaging and is still rather limited in scope. Relevant recent studies are summarized in Table 4. In brief, PD has been associated with regional reductions in CBF as well as prolonged arterial-transit time (ATT). However, there has yet to be a consensus regarding the extent of hypoperfusion in PD, likely due to disease variability across patients and the limited scope of application.

Amyotrophic lateral sclerosis

ALS is diagnosed based on symptoms of muscle weakness or twitching, slurred speech, or trouble with physical tasks. The most common form of ALS is "sporadic ALS", implying that the pathology is independent of gender, ethnicity and age. Nonetheless, afflicted individuals are most often aged between 40 and 60 years, making ALS an aging-sensitive disease. Histological evidence suggests that like FTD, ALS is characterized by frontal-lobe degeneration (Zago et al., 2011). More recently, ALS and FTD are found to be closely related conditions with overlapping clinical, pathological, radiological, and genetic characteristics (Zago et al., 2011). While MRI has been used to assess brain function (Lulé et al., 2009) and structure (Turner and Modo, 2010) in ASL, the use of MRI to assess brain physiology has yet to develop, constituting a promising area of expanded application.

Table 4
Functional MRI in physiological imaging of Parkinson's disease: select human studies.

Reference	Cohort and Technique	Findings
(Kamagata et al., 2011)	35 PD, 11 PD with dementia and 35 older controls; CBF measured using PASL at 3 T	Both PD and PD-dementia groups showed lower CBF in posterior cortex than controls.
(Al-Bachari et al., 2017)	14 PD and 14 older controls; CBF and ATT measured using PASL at 3 T	CBF in PD significantly correlated with cognitive assessment, and ATT in PD was significantly prolonged across the brain. However, no CBF difference between PD and controls was found.

Future challenges and opportunities

Interpretation

While a comprehensive view of brain physiology is critical for understanding disease processes, it must be borne in mind that every imaging technique discussed in this review is associated with specific assumptions. For instance, whether using BOLD or perfusion-based fMRI methods, the measurement of neural response depends on intact neurovascular coupling. Moreover, as described in earlier sections, the chemical mechanisms of neurally induced and CO_2-induced hyperemia are not entirely the same. Thus, the interpretation of functional measurements based on the knowledge of CVR in the presence of compromised neurovascular coupling may be misleading. This issue directly impacts CO_2-calibrated fMRI, leading to possible biases in $CMRO_2$ estimation. As another example, contrast-enhanced perfusion quantification models assume an intact BBB. While ASL methods are relatively immune to BBB leakage, the prolonged arterial transit times (particularly in the occipital lobe) in older participants and those with brain disorders will likely lead to CBF underestimation in a spatially heterogeneous manner. Finally, while it is tempting to exploit resting-state fMRI for physiological measurements (Kannurpatti et al., 2011; Liu et al., 2017; Makedonov et al., 2016), the origins of the resting-state data are time-variant and far from being fully understood, making accurate interpretation even more challenging.

Furthermore, most fMRI methods are negatively affected by the presence of susceptibility artifacts obscuring medial temporal regions, which are key regions affected by both aging and most forms of dementia. Specifically, the signal dropouts in these regions lead to artifactual underestimations of fMRI activation and perfusion, impeding meaningful evaluations of physiological health.

Clinical translation and large-scale data gathering

It is evident, from this review, that the vast majority of studies addressing brain physiology in age-related neurodegenerative diseases focus on perfusion mapping alone. This is likely due to (1) the relatively high interpretability of CBF maps; (2) the ease of quantitative perfusion mapping using ASL. However, ASL has yet to reach its full potential, not only due to potential acquisition challenges in the clinical realm (Alsop et al., 2014), but also due to the lack of a standard, plug-and-play post-processing pipeline (Essig et al., 2013).

Beyond perfusion mapping, in terms of gathering more comprehensive physiological data on a routine basis, the following challenges need to be met.

(1) *High demand for patient compliance.* As a case in point, the use of hypercapnic manipulation for CVR mapping in AD patients and elderly participants are non-trivial, neither is breath-holding is not without its difficulties. The high failure rate in CVR mapping amongst older adults and patients (31% in CO_2-inhalation studies (Cantin et al., 2011) and 21% in breath-holding studies (Jahanian et al., 2017) attests to this translational challenge.
(2) *Long imaging time.* The preparation of a typical CVR scan (including necessary patient training and instrumentation set up) may take 30 min, not ideal for the incorporation of such scans in clinical and large-scale studies. Even the more established DSC MRI scans for mapping BBB permeability make take up to 25 min (van de Haar et al., 2016), posing a serious challenge for routine adoption.
(3) *High technical demand.* The successful use of techniques such as qBOLD, QUIXOTIC and QSM requires considerable technical understanding and expertise. For the most part, even more established methods such as calibrated fMRI involves a series of experiments that not only require experienced research staff but also custom data analysis. The availability of the necessary expertise is still relatively limited, which is even more the case for CBV and OEF mapping. Thus, novel imaging methods must follow their development cycle to transform from "boutique" techniques into those suitable for clinical translation, and such cycles may take decades.

The need for larger-scale data gathering implies that the imaging techniques employed need to be accessible, non-invasive, cost effective as well as undemanding for participants and experimenters. These requirements may in fact present an opportunity for the expanded use of resting-state based approaches (Christen et al., 2015; Golestani et al., 2016; Jahanian et al., 2017; Liu et al., 2017). While resting-state CVR methods are mostly non-quantitative and do not provide equivalent amounts of information as measurements based on gas challenges, researchers have to assess the utility of quantitative versus qualitative measurements in view of practical challenges in carrying out measurements.

"Better" imaging – study size versus complexity

There is no doubt that MRI physicists must work more closely with front-line clinical researchers as well as physicists from other imaging domains to accelerate the translation of some of the more novel techniques. In order to maximize data efficiency, these translational efforts must be coordinated with the vast amounts of data being made available worldwide through large-scale multi-site research studies. That is, although we can always increase the sample size or comprehensiveness of the image acquisitions, it is more imperative at this time to find new ways to extract novel information from routine imaging data sets rather than rely on more technically-complex data acquisitions. Moreover, to enhance the knowledge gained through these immense neuroimaging databanks, the value of multi-modal data fusion should be better capitalized in studying brain physiology. There is an increasing need to associate fMRI findings with those of structural (anatomical, diffusion-tensor imaging and so on) and metabolic imaging (MRS) to gain valuable perspective. As a case in point, the observation of age-related CBF changes must be interpreted in light of concurrent brain atrophy.

Conversely, not all research questions are best addressed using immense data sets. There is unique value to designing multimodal imaging protocols. That is, fMRI methods do not have to be used in isolation, but can be combined with methods such as EEG, TCD and NIRS (Fabiani et al., 2014) to achieve more comprehensive and less biased characterizations of the neurovascular system.

The quest for potential biomarkers

The term "biomarker" is used widely to suggest potential uses of new fMRI methods. A biomarker is defined as "a characteristic that is objectively measured and evaluated as an indicator of normal biological processes, pathological processes, or pharmacological responses to a therapeutic intervention" (Biomarkers Definitions Working Group., 2001). Three aspects of biomarker validity has been suggested (Schulte and Perera, 2012): 1) content validity, which shows the degree to which a biomarker reflects the biological phenomenon studied, 2) construct validity, which pertains to other relevant characteristics of the disease or trait, and 3) criterion validity, which shows the extent to which the biomarker correlates with the specific disease and is usually measured by sensitivity, specificity and predictive power. Thus, although the sensitivity and reproducibility of an imaging measure are often used to validate it as a biomarker, it would be premature to do so based on these aspects alone.

In terms of physiological fMRI, great strides have been taken in ascertaining the sensitivity, specificity and predictive power of metrics such as ASL perfusion. Despite the dependence on group effects and discrepancies in subject categorization, it is generally recognized that CBF is a biomarker of neurodegeneration (Hays et al., 2016). However,

CBF still lacks specificity to underlying biological mechanisms, as it reflects both vascular and neuronal information. To overcome this limitation, the next frontier for biomarker development in the fMRI context should ideally be CVR and resting $CMRO_2$. These metrics are ripe for large-scale validation for biomarker attributes, as they are becoming increasingly established as traits as well as less demanding in terms of burden on patients.

Brain-body connection

In the quest for imaging biomarkers for neurodegeneration, the connection between the brain and whole-body physiology cannot be overlooked. As cardiovascular and metabolic diseases (such as hypertension and diabetes) are major modifiable risk factors of age-related neurodegeneration (Girouard and Iadecola, 2006), it is likely that systemic vascular dysfunction is an integral part of the disease mechanism. Indeed, the prevalence of these systemic diseases is blurring the traditional diagnostic categorizations across neurodegenerative disease (such as CAA, AD and VaD) (Iadecola, 2004). As the main ultimate aims of physiological brain imaging is to use physiological knowledge to prognose disease and monitor treatment outcomes, it is likely that neuronal pathogenesis and regeneration will need to be interpreted in terms of modulatory effects originating from outside the brain.

References

Agbangla, N.F., Audiffren, M., Albinet, C.T., 2017. Use of near-infrared spectroscopy in the investigation of brain activation during cognitive aging: a systematic review of an emerging area of research. Ageing Res. Rev. 38, 52–66.

Ainslie, P.N., Duffin, J., 2009. Integration of cerebrovascular CO2 reactivity and chemoreflex control of breathing: mechanisms of regulation, measurement, and interpretation. Aust. J. Pharm.: Regulatory, Integrative and Comparative Physiology 296, R1473–R1495.

Akgören, N., Dalgaard, P., Lauritzen, M., 1996. Cerebral blood flow increases evoked by electrical stimulation of rat cerebellar cortex: relation to excitatory synaptic activity and nitric oxide synthesis. Brain Res. 710, 204–214.

Al-Bachari, S., Vidyasagar, R., Emsley, H.C., Parkes, L.M., 2017. Structural and physiological neurovascular changes in idiopathic Parkinson's disease and its clinical phenotypes. J. Cerebr. Blood Flow Metabol. 271678X16688919.

Alsop, D.C., Detre, J.A., Grossman, M., 2000. Assessment of cerebral blood flow in Alzheimer's disease by spin-labeled magnetic resonance imaging. Ann. Neurol. 47, 93–100.

Alsop, D.C., Detre, J.A., Golay, X., Gunther, M., Hendrikse, J., Hernandez-Garcia, L., Lu, H., Macintosh, B.J., Parkes, L.M., Smits, M., van Osch, M.J., Wang, D.J., Wong, E.C., Zaharchuk, G., 2014. Recommended implementation of arterial spin-labeled perfusion MRI for clinical applications: a consensus of the ISMRM perfusion study group and the European consortium for ASL in dementia. Magn. Reson. Med. Epub ahead of print, Apr. 2014. https://doi.org/10.1002/mrm.25197.

Amor, S., Puentes, F., Baker, D., van der Valk, P., 2010. Inflammation in neurodegenerative diseases. Immunology 129, 154–169.

Ances, B.M., Liang, C.L., Leontiev, O., Perthen, J.E., Fleisher, A.S., Lansing, A.E., Buxton, R.B., 2009. Effects of aging on cerebral blood flow, oxygen metabolism, and blood oxygenation level dependent responses to visual stimulation. Hum. Brain Mapp. 30, 1120–1132.

Archer, H.A., Smailagic, N., John, C., Holmes, R.B., Takwoingi, Y., Coulthard, E.J., Cullum, S., 2015. Regional cerebral blood flow single photon emission computed tomography for detection of Frontotemporal dementia in people with suspected dementia. Cochrane Database Syst. Rev. CD010896.

Artero, S., Tiemeier, H., Prins, N.D., Sabatier, R., Breteler, M.M.B., Ritchie, K., 2004. Neuroanatomical localisation and clinical correlates of white matter lesions in the elderly. J. Neurol. Neurosurg. Psychiatry 75, 1304–1308.

Aslan, S., Xu, F., Wang, P.L., Uh, J., Yezhuvath, U.S., van Osch, M., Lu, H., 2010. Estimation of labeling efficiency in pseudocontinuous arterial spin labeling. Magn. Reson. Med. 63, 765–771.

Asllani, I., Habeck, C., Scarmeas, N., Borogovac, A., Brown, T.R., Stern, Y., 2008. Multivariate and univariate analysis of continuous arterial spin labeling perfusion MRI in Alzheimer's disease. J. Cerebr. Blood Flow Metabol. 28, 725–736.

Attwell, D., Laughlin, S.B., 2001. An energy budget for signaling in the grey matter of the brain. J. Cerebr. Blood Flow Metabol. 21, 1133–1145.

Bangen, K.J., Restom, K., Liu, T.T., Jak, A.J., Wierenga, C.E., Salmon, D.P., Bondi, M.W., 2009. Differential age effects on cerebral blood flow and BOLD response to encoding: associations with cognition and stroke risk. Neurobiol. Aging 30, 1276–1287.

Bangen, K.J., Restom, K., Liu, T.T., Wierenga, C.E., Jak, A.J., Salmon, D.P., Bondi, M.W., 2012. Assessment of Alzheimer's disease risk with functional magnetic resonance imaging: an arterial spin labeling study. J. Alzheimers. Dis. 31 (Suppl. 3), S59–S74.

Barbier, E.L., Lamalle, L., Décorps, M., 2001. Methodology of brain perfusion imaging. J. Magn. Reson. Imag. 13, 496–520.

Barbier, E.L., St Lawrence, K.S., Grillon, E., Koretsky, A.P., Décorps, M., 2002. A model of blood-brain barrier permeability to water: accounting for blood inflow and longitudinal relaxation effects. Magn. Reson. Med. 47, 1100–1109.

Barker, P.B., Golay, X., Zaharchuk, G., 2013. Clinical Perfusion MRI: Techniques and Applications. Cambridge University Press.

Baron, J.C., Marchal, G., 1992. Cerebral and cardiovascular aging and brain energy metabolism. Studies with positron-emission tomography in man. Presse Med. 21, 1231–1237.

Bartelle, B.B., Barandov, A., Jasanoff, A., 2016. Molecular fMRI. J. Neurosci. 36, 4139–4148.

Battisti-Charbonney, A., Fisher, J., Duffin, J., 2011. The cerebrovascular response to carbon dioxide in humans. J physiology 589, 3039–3048.

Bell, R.D., Zlokovic, B.V., 2009. Neurovascular mechanisms and blood-brain barrier disorder in Alzheimer's disease. Acta Neuropathol. 118, 103–113.

Bell, R.D., Winkler, E.A., Sagare, A.P., Singh, I., LaRue, B., Deane, R., Zlokovic, B.V., 2010. Pericytes control key neurovascular functions and neuronal phenotype in the adult brain and during brain aging. Neuron 68, 409–427.

Belliveau, J.W., Kennedy, D.N., McKinstry, R.C., Buchbinder, B.R., Weisskoff, R.M., Cohen, M.S., Vevea, J.M., Brady, T.J., Rosen, B.R., 1991. Functional mapping of the human visual cortex by magnetic resonance imaging. Science 254, 716–719.

Bergers, G., Song, S., 2005. The role of pericytes in blood-vessel formation and maintenance. Neuro Oncol. 7, 452–464.

Bertrand, P., Poirier, J., Oda, T., Finch, C.E., Pasinetti, G.M., 1995. Association of apolipoprotein E genotype with brain levels of apolipoprotein E and apolipoprotein J (clusterin) in Alzheimer disease. Mol. Brain Res. 33, 174–178.

Binnewijzend, M.A.A., Kuijer, J.P.A., van der Flier, W.M., Benedictus, M.R., Möller, C.M., Pijnenburg, Y.A.L., Lemstra, A.W., Prins, N.D., Wattjes, M.P., van Berckel, B.N.M., Scheltens, P., Barkhof, F., 2014. Distinct perfusion patterns in Alzheimer's disease, frontotemporal dementia and dementia with Lewy bodies. Eur. Radiol. 24, 2326–2333.

Biomarkers Definitions Working Group, 2001. Biomarkers and surrogate endpoints: preferred definitions and conceptual framework. Clin. Pharmacol. Ther. 69, 89–95.

Black, S., Gao, F., Bilbao, J., 2009. Understanding white matter disease: imaging-pathological correlations in vascular cognitive impairment. Stroke 40, S48–S52.

Blennow, K., de Leon, M.J., Zetterberg, H., 2006. Alzheimer's disease. Lancet 368, 387–403.

Blockley, N.P., Driver, I.D., Francis, S.T., Fisher, J.A., Gowland, P.A., 2011. An improved method for acquiring cerebrovascular reactivity maps. Magn. Reson. Med. 65, 1278–1286.

Blockley, N.P., Griffeth, V.E.M., Simon, A.B., Dubowitz, D.J., Buxton, R.B., 2015. Calibrating the BOLD response without administering gases: comparison of hypercapnia calibration with calibration using an asymmetric spin echo. Neuroimage 104, 423–429.

Blockley, N.P., Harkin, J.W., Bulte, D.P., 2017. Rapid cerebrovascular reactivity mapping: enabling vascular reactivity information to be routinely acquired. Neuroimage 159, 214–223.

Bolar, D.S., Rosen, B.R., Sorensen, A.G., Adalsteinsson, E., 2011. QUantitative Imaging of eXtraction of oxygen and TIssue consumption (QUIXOTIC) using venular-targeted velocity-selective spin labeling. Magn. Reson. Med. 66, 1550–1562.

Bookheimer, S., Burggren, A., 2009. APOE-4 genotype and neurophysiological vulnerability to Alzheimer's and cognitive aging. Annu. Rev. Clin. Psychol. 5, 343–362.

Boumezbeur, F., Mason, G.F., de Graaf, R.A., Behar, K.L., Cline, G.W., Shulman, G.I., Rothman, D.L., Petersen, K.F., 2010. Altered brain mitochondrial metabolism in healthy aging as assessed by in vivo magnetic resonance spectroscopy. J. Cerebr. Blood Flow Metabol. 30, 211–221.

Brenner, S.R., 2008. Neurovascular unit dysfunction: a vascular component of alzheimer disease? Neurology 70, 243–244.

Brettschneider, J., Del Tredici, K., Lee, V.M.-Y., Trojanowski, J.Q., 2015. Spreading of pathology in neurodegenerative diseases: a focus on human studies. Nat. Rev. Neurosci. 16, 109–120.

Bright, M.G., Murphy, K., 2013. Reliable quantification of BOLD fMRI cerebrovascular reactivity despite poor breath-hold performance. Neuroimage 83, 559–568.

Bright, M.G., Bulte, D.P., Jezzard, P., Duyn, J.H., 2009. Characterization of regional heterogeneity in cerebrovascular reactivity dynamics using novel hypocapnia task and BOLD fMRI. Neuroimage 48, 166–175.

Bron, E.E., Steketee, R.M.E., Houston, G.C., Oliver, R.A., Achterberg, H.C., Loog, M., van Swieten, J.C., Hammers, A., Niessen, W.J., Smits, M., Klein, S., Alzheimer's Disease Neuroimaging Initiative, 2014. Diagnostic classification of arterial spin labeling and structural MRI in presenile early stage dementia. Hum. Brain Mapp. 35, 4916–4931.

Brugniaux, J.V., Hodges, A.N., Hanly, P.J., Poulin, M.J., 2007. Cerebrovascular responses to altitude. Respir. Physiol. Neurobiol. 158, 212–223.

Buratti, L., Balestrini, S., Altamura, C., Viticchi, G., Falsetti, L., Luzzi, S., Provinciali, L., Vernieri, F., Silvestrini, M., 2015. Markers for the risk of progression from mild cognitive impairment to Alzheimer's disease. J. Alzheimers. Dis 45, 883–890.

Buxton, R.B., Frank, L.R., 1997. A model for the coupling between cerebral blood flow and oxygen metabolism during neural stimulation. J. Cerebr. Blood Flow Metabol. 17, 64–72.

Buxton, R.B., Frank, L.R., Wong, E.C., Siewert, B., Warach, S., Edelman, R.R., 1998. A general kinetic model for quantitative perfusion imaging with arterial spin labelling. Magn. Reson. Med. 40, 383–396.

Cantin, S., Villien, M., Moreaud, O., Tropres, I., Keignart, S., Chipon, E., Le Bas, J.-F., Warnking, J., Krainik, A., 2011. Impaired cerebral vasoreactivity to CO2 in Alzheimer's disease using BOLD fMRI. Neuroimage 58, 579–587.

Cauli, B., Tong, X.-K., Rancillac, A., Serluca, N., Lambolez, B., Rossier, J., Hamel, E., 2004. Cortical GABA interneurons in neurovascular coupling: relays for subcortical vasoactive pathways. J. Neurosci. 24, 8940–8949.
Charidimou, A., Boulouis, G., Pasi, M., Auriel, E., van Etten, E.S., Haley, K., Ayres, A., Schwab, K.M., Martinez-Ramirez, S., Goldstein, J.N., Rosand, J., Viswanathan, A., Greenberg, S.M., Gurol, M.E., 2017. MRI-visible perivascular spaces in cerebral amyloid angiopathy and hypertensive arteriopathy. Neurology 88, 1157–1164.
Chen, J.J., Pike, G.B., 2010. Global cerebral oxidative metabolism during hypercapnia and hypocapnia in humans: implications for BOLD fMRI. J. Cerebr. Blood Flow Metabol. 30, 1094–1099.
Chen, J.J., Smith, M.R., Frayne, R., 2005. The impact of partial-volume effects in dynamic susceptibility contrast magnetic resonance perfusion imaging. J. Magn. Reson. Imag. 22, 390–399.
Chen, A., Shyr, M.-H., Chen, T.-Y., Lai, H.-Y., Lin, C.-C., Yen, P.-S., 2006. Dynamic CT perfusion imaging with acetazolamide challenge for evaluation of patients with unilateral cerebrovascular steno-occlusive disease. AJNR Am. J. Neuroradiol 27, 1876–1881.
Chen, J.J., Wieckowska, M., Meyer, E., Pike, G.B., 2008. Cerebral blood flow measurement using fMRI and PET: a cross-validation study. Int. J. Biomed. Imag. 2008, 516359.
Chen, J.J., Rosas, H.D., Salat, D.H., 2011. Age-associated reductions in cerebral blood flow are independent from regional atrophy. Neuroimage 55, 468–478.
Chen, J.J., Rosas, H.D., Salat, D.H., 2013. The relationship between cortical blood flow and sub-cortical white-matter health across the adult age span. PLoS One 8, e56733.
Chiarelli, P.A., Bulte, D.P., Wise, R., Gallichan, D., Jezzard, P., 2007a. A calibration method for quantitative BOLD fMRI based on hyperoxia. Neuroimage 37, 808–820.
Chiarelli, P.A., Bulte, D.P., Wise, R., Gallichan, D., Jezzard, P., 2007b. A calibration method for quantitative BOLD fMRI based on hyperoxia. Neuroimage 37, 808–820.
Chow, N., Bell, R.D., Deane, R., Streb, J.W., Chen, J., Brooks, A., Van Nostrand, W., Miano, J.M., Zlokovic, B.V., 2007. Serum response factor and myocardin mediate arterial hypercontractility and cerebral blood flow dysregulation in Alzheimer's phenotype. Proc. Natl. Acad. Sci. U. S. A 104, 823–828.
Christen, T., Jahanian, H., Ni, W.W., Qiu, D., Moseley, M.E., Zaharchuk, G., 2015. Noncontrast mapping of arterial delay and functional connectivity using resting-state functional MRI: a study in Moyamoya patients. J. Magn. Reson. Imag. 41, 424–430.
Cohen, E.R., Rostrup, E., Sidaros, K., Lund, T.E., Paulson, O.B., Ugurbil, K., Kim, S.G., 2004. Hypercapnic normalization of BOLD fMRI: comparison across field strengths and pulse sequences. Neuroimage 23, 613–624.
Dai, W., Garcia, D., De Bazelaire, C., Alsop, D.C., 2008. Continuous flow-driven inversion for arterial spin labeling using pulsed radio frequency and gradient fields. Magn. Reson. Med. 60, 1488–1497.
Davis, T.L., Kwong, K.K., Weisskoff, R.M., Rosen, B.R., 1998. Calibrated functional MRI: mapping the dynamics of oxidative metabolism. Proc. Natl. Acad. Sci. U. S. A 95, 1834–1839.
de la Torre, J.C., 2010. Vascular risk factor detection and control may prevent Alzheimer's disease. Ageing Res. Rev. 9, 218–225.
de la Torre, J.C., 2016. Cerebral perfusion enhancing interventions: a new strategy for the prevention of alzheimer dementia. Brain Pathol. 26, 618–631.
de la Torre, J.C., Mussivand, T., 1993. Can disturbed brain microcirculation cause Alzheimer's disease? Neurol. Res. 15, 146–153.
Dekoninck, W.J., Piraux, A., Uytdenhoef, P., Jacquy, J., 1982. Relationship between EEG and cerebral blood flow in normal brain aging. In: Experimental Brain Research Supplementum, pp. 208–215.
Detre, J.A., Alsop, D.C., 1999. Perfusion magnetic resonance imaging with continuous arterial spin labeling: methods and clinical applications in the central nervous system. Eur. J. Radiol. 30, 115–124.
Detre, J.A., Leigh, J.S., Williams, D.S., Koretsky, A.P., 1992. Perfusion imaging. Magn. Reson. Med. 23, 37–45.
Donahue, M.J., van Laar, P.J., van Zijl, P.C.M., Stevens, R.D., Hendrikse, J., 2009. Vascular space occupancy (VASO) cerebral blood volume-weighted MRI identifies hemodynamic impairment in patients with carotid artery disease. J. Magn. Reson. Imag. 29, 718–724.
Dormehl, I.C., Jordaan, B., Oliver, D.W., Croft, S., 1999. SPECT monitoring of improved cerebral blood flow during long-term treatment of elderly patients with nootropic drugs. Clin. Nucl. Med. 24, 29–34.
Drubach, D., 2000. The Brain Explained. Prentice Hall.
Du, A.T., Jahng, G.H., Hayasaka, S., Kramer, J.H., Rosen, H.J., Gorno-Tempini, M.L., Rankin, K.P., Miller, B.L., Weiner, M.W., Schuff, N., 2006. Hypoperfusion in frontotemporal dementia and Alzheimer disease by arterial spin labeling MRI. Neurology 67, 1215–1220.
Dugger, B.N., Dickson, D.W., 2017. Pathology of neurodegenerative diseases. Cold spring harb. Perspect. Biol. 9. https://doi.org/10.1101/cshperspect.a028035.
Duling, B.R., Berne, R.M., 1970. Longitudinal gradients in periarteriolar oxygen tension: a possible mechanism for the participation of oxygen in local regulation of blood flow. Circ. Res. 27, 669–678.
Dumas, A., Dierksen, G.A., Gurol, M.E., Halpin, A., Martinez-Ramirez, S., Schwab, K., Rosand, J., Viswanathan, A., Salat, D.H., Polimeni, J.R., Greenberg, S.M., 2012. Functional magnetic resonance imaging detection of vascular reactivity in cerebral amyloid angiopathy. Ann. Neurol. 72, 76–81.
D'Esposito, M., Deouell, L.Y., Gazaley, A., 2003. Alterations in the BOLD fMRI signal with ageing and disease: a challenge for neuroimaging. Nat. Rev. Neurosci. 4, 863–872.
Erickson, M.A., Banks, W.A., 2013. Blood–brain barrier dysfunction as a cause and consequence of Alzheimer's disease. J. Cerebr. Blood Flow Metabol. 33, 1500–1513.
Essig, M., Shiroishi, M.S., Nguyen, T.B., Saake, M., Provenzale, J.M., Enterline, D., Anzalone, N., Dörfler, A., Rovira, A., Wintermark, M., Law, M., 2013. Perfusion MRI: the five most frequently asked technical questions. AJR Am. J. Roentgenol. 200, 24–34.
Fabiani, M., Gordon, B.A., Maclin, E.L., Pearson, M.A., Brumback-Peltz, C.R., Low, K.A., McAuley, E., Sutton, B.P., Kramer, A.F., Gratton, G., 2014. Neurovascular coupling in normal aging: a combined optical, ERP and fMRI study. Neuroimage 85 Pt 1, 592–607.
Fan, A.P., Benner, T., Bolar, D.S., Rosen, B.R., Adalsteinsson, E., 2012. Phase-based regional oxygen metabolism (PROM) using MRI. Magn. Reson. Med. 67, 669–678.
Fierstra, J., Sobczyk, O., Battisti-Charbonney, A., Mandell, D.M., Poublanc, J., Crawley, A.P., Mikulis, D.J., Duffin, J., Fisher, J.A., 2013. Measuring cerebrovascular reactivity: what stimulus to use? J. Physiol. 591, 5809–5821.
Fjell, A.M., Westlye, L.T., Amlien, I., Espeseth, T., Reinvang, I., Raz, N., Agartz, I., Salat, D.H., Greve, D.N., Fischl, B., Dale, A.M., Walhovd, K.B., 2009. High consistency of regional cortical thinning in aging across multiple samples. Cerebr. Cortex 19, 2001–2012.
Fox, P.T., Raichle, M.E., 1986. Focal physiological uncoupling of cerebral blood flow and oxidative metabolism during somatorsensory stimulation in human subjects. Proc. Natl. Acad. Sci. U. S. A 83, 1140–1144.
Frahm, J., Baudewig, J., Kallenberg, K., Kastrup, A., Dietmar Merboldt, K., Dechent, P., 2008. The post-stimulation undershoot in BOLD fMRI of human brain is not caused by elevated cerebral blood volume. Neuroimage 40, 473–481.
Gao, Y.-Z., Zhang, J.-J., Liu, H., Wu, G.-Y., Xiong, L., Shu, M., 2013. Regional cerebral blood flow and cerebrovascular reactivity in Alzheimer's disease and vascular dementia assessed by arterial spinlabeling magnetic resonance imaging. Curr. Neurovascular Res. 10, 49–53.
Gauthier, C.J., Hoge, R.D., 2012. Magnetic resonance imaging of resting OEF and $CMRO_2$ using a generalized calibration model for hypercapnia and hyperoxia. Neuroimage 60, 1212–1225.
Gauthier, C.J., Madjar, C., Desjardins-Crépeau, L., Bellec, P., Bherer, L., Hoge, R.D., 2012. Age dependence of hemodynamic response characteristics in human functional magnetic resonance imaging. Neurobiol. Aging. https://doi.org/10.1016/j.neurobiolaging.2012.11.002.
Girouard, H., Iadecola, C., 2006. Neurovascular coupling in the normal brain and in hypertension, stroke, and Alzheimer disease. J. Appl. Physiol. 100, 328–335.
Gjedde, A., Marrett, S., Vafaee, M., 2002. Oxidative and nonoxidative metabolism of excited neurons and astrocytes. J. Cerebr. Blood Flow Metabol. 22, 1–14.
Glodzik, L., Randall, C., Rusinek, H., de Leon, M.J., 2013. Cerebrovascular reactivity to carbon dioxide in Alzheimer's disease. J. Alzheimers. Dis 35, 427–440.
Golestani, A.M., Wei, L.L., Chen, J.J., 2016. Quantitative mapping of cerebrovascular reactivity using resting-state BOLD fMRI: validation in healthy adults. Neuroimage 138, 147–163.
Gomez-Isla, T., Hollister, R., West, H., Mui, S., Growdon, J.H., Pelersen, R.C., Parisi, J.E., Hyman, B.T., 1996. Neuronal loss in alzheimer's disease. J. Neuropathol. Exp. Neurol. 55, 617.
Gorelick, P.B., 2004. Risk factors for vascular dementia and Alzheimer disease. Stroke 35, 2620–2622.
Grandin, C., Bol, A., Smith, A., Michel, C., Cosnard, G., 2005. Absolute CBF and CBV measurements by MRI bolus tracking before and after acetazolamide challenge: repeatabilily and comparison with PET in humans. Neuroimage. https://doi.org/10.1016/j.neuroimage.2005.02.028.
Grubb, R.L., Phelps, M.E., Eichling, J.O., 1974. The effects of vascular changes in PaCO2 on cerebral blood volume, blood flow and vascular mean transit time. Stroke 5, 630–639.
Gupta, A., Nair, S., Schweitzer, A.D., Kishore, S., Johnson, C.E., Comunale, J.P., Tsiouris, A.J., Sanelli, P.C., 2012. Neuroimaging of cerebrovascular disease in the aging brain. Aging Dis 3, 414–425.
Haacke, E.M., Lai, S., Reichenbach, J.R., Kupusamy, K., Hoogenraad, F.G.C., Takeichi, H., Lin, W., 1997. Vivo Measurement of Blood Oxygen Saturation Using Magnetic Resonance Imaging: a Direct Validation of the Blood Oxygen Level-dependent Concept in Functional Brain Imaging, vol. 5, pp. 341–346.
Hajjar, I., Sorond, F., Lipsitz, L.A., 2015. Apolipoprotein E, carbon dioxide vasoreactivity, and cognition in older adults: effect of hypertension. J. Am. Geriatr. Soc. 63, 276–281.
Halani, S., Kwinta, J.B., Golestani, A.M., Khatamian, Y.B., Chen, J.J., 2015. Comparing cerebrovascular reactivity measured using BOLD and cerebral blood flow MRI: the effect of basal vascular tension on vasodilatory and vasoconstrictive reactivity. Neuroimage 110, 110–123.
Hamel, E., 2004. Cholinergic modulation of the cortical microvascular bed. Prog. Brain Res. 145, 171–178.
Han, P.K., Choi, S.H., Park, S.-H., 2016. Investigation of control scans in pseudo-continuous arterial spin labeling (pCASL): strategies for improving sensitivity and reliability of pCASL. Magn. Reson. Med. 78, 917–929.
Hashimura, T., Kimura, T., Miyakawa, T., 1991. Morphological changes of blood vessels in the brain with Alzheimer's disease. Jpn. J. Psychiatry Neurol. 45, 661–665.
Hayashi, T., Watabe, H., Kudomi, N., Kim, K.M., Enmi, J.-I., Hayashida, K., Iida, H., 2003. A theoretical model of oxygen delivery and metabolism for physiologic interpretation of quantitative cerebral blood flow and metabolic rate of oxygen. J. Cerebr. Blood Flow Metabol. 23, 1314–1323.
Hays, C.C., Zlatar, Z.Z., Wierenga, C.E., 2016. The utility of cerebral blood flow as a biomarker of preclinical Alzheimer's disease. Cell. Mol. Neurobiol. 36, 167–179.
He, X., Zhu, M., Yablonskiy, D.A., 2008. Validation of oxygen extraction fraction measurement by qBOLD technique. Magn. Reson. Med. 60, 882–888.
Heffernan, K.S., Jae, S.Y., Lee, M., Woods, J.A., Fernhall, B., 2008. Arterial wave reflection and vascular autonomic modulation in young and older men. Aging Clin. Exp. Res. 20, 1–7.

Herzig, M.C., Van Nostrand, W.E., Jucker, M., 2006. Mechanism of cerebral beta-amyloid angiopathy: murine and cellular models. Brain Pathol. 16, 40–54.
Herzig, R., Hlustík, P., Skoloudík, D., Sanák, D., Vlachová, I., Herman, M., Kanovský, P., 2008. Assessment of the cerebral vasomotor reactivity in internal carotid artery occlusion using a transcranial Doppler sonography and functional MRI. J. Neuroimaging 18, 38–45.
Heye, A.K., Culling, R.D., Valdés Hernández, M.D.C., Thrippleton, M.J., Wardlaw, J.M., 2014. Assessment of blood-brain barrier disruption using dynamic contrast-enhanced MRI. A systematic review. Neuroimage Clin 6, 262–274.
Hirao, K., Ohnishi, T., Hirata, Y., Yamashita, F., Mori, T., Moriguchi, Y., Matsuda, H., Nemoto, K., Imabayashi, E., Yamada, M., Iwamoto, T., Arima, K., Asada, T., 2005. The prediction of rapid conversion to Alzheimer's disease in mild cognitive impairment using regional cerebral blood flow SPECT. Neuroimage 28, 1014–1021.
Hoge, R.D., 2012. Calibrated fMRI. Neuroimage 62, 930–937.
Hoge, R.D., Atkinson, J., Gill, B., Crelier, G.R., Marrett, S., Pike, G.B., 1999. Investigation of BOLD signal dependence on CBF and CMRO: the deoxyhemoglobin dilution model. In: Presented at the Proceeding of the Fifth International Conference on Functional Mapping of the Human Brain.
Hua, J., Qin, Q., Pekar, J.J., van Zijl, P.C.M., 2011. Measurement of absolute arterial cerebral blood volume in human brain without using a contrast agent. NMR Biomed. 24, 1313–1325.
Hua, J., Liu, P., Kim, T., Donahue, M., Rane, S., Jean Chen, J., Qin, Q., Kim, S.-G., 2018. MRI techniques to measure arterial and venous cerebral blood volume. Neuroimage. https://doi.org/10.1016/j.neuroimage.2018.02.027.
Iadecola, C., 2004. Neurovascular regulation in the normal brain and in Alzheimer's disease. Nat. Rev. Neurosci. 5, 347–360.
Iadecola, C., Pelligrino, D.A., Moskowitz, M.A., Lassen, N.A., 1994. Nitric oxide synthase inhibition and cerebrovascular regulation. J. Cerebr. Blood Flow Metabol. 14, 175–192.
Iannetti, G.D., Wise, R.G., 2007. BOLD functional MRI in disease and pharmacological studies: room for improvement? Magn. Reson. Imaging 25, 978–988.
Ibáñez, V., Pietrini, P., Furey, M.L., Alexander, G.E., Millet, P., Bokde, A.L.W., Teichberg, D., Schapiro, M.B., Horwitz, B., Rapoport, S.I., 2004. Resting state brain glucose metabolism is not reduced in normotensive healthy men during aging, after correction for brain atrophy. Brain Res. Bull. 63, 147–154.
Ishii, K., Mori, E., Kitagaki, H., Sakamoto, S., Yamaji, S., Imamura, T., Ikejiri, Y., Kono, M., 1996. The clinical utility of visual evaluation of scintigraphic perfusion patterns for Alzheimer's disease using I-123 IMP SPECT. Clin. Nucl. Med. 21, 106–110.
Ito, H., Takahashi, K., Hatazawa, J., Kim, S.-G., Kanno, I., 2001. Changes in human regional cerebral blood flow and cerebral blood volume during visual stimulation measured by positron emission tomography. J. Cerebr. Blood Flow Metabol. 21, 608–612.
Jagust, W., Reed, B., Mungas, D., Ellis, W., Decarli, C., 2007. What does fluorodeoxyglucose PET imaging add to a clinical diagnosis of dementia? Neurology 69, 871–877.
Jahanian, H., Christen, T., Moseley, M.E., Pajewski, N.M., Wright, C.B., Tamura, M.K., Zaharchuk, G., SPRINT Study Research Group, 2017. Measuring vascular reactivity with resting-state blood oxygenation level-dependent (BOLD) signal fluctuations: a potential alternative to the breath-holding challenge? J. Cerebr. Blood Flow Metabol. 37, 2526–2538.
Jain, V., Langham, M.C., Floyd, T.F., Jain, G., Magland, J.F., Wehrli, F.W., 2011. Rapid magnetic resonance measurement of global cerebral metabolic rate of oxygen consumption in humans during rest and hypercapnia. J. Cerebr. Blood Flow Metabol. 31, 1504–1512.
Jain, V., Duda, J., Avants, B., Giannetta, M., Xie, S.X., Roberts, T., Detre, J.A., Hurt, H., Wehrli, F.W., Wang, D.J.J., 2012. Longitudinal reproducibility and accuracy of pseudo-continuous arterial spin-labeled perfusion MR imaging in typically developing children. Radiology 263, 527–536.
Jellinger, K.A., 2007. The enigma of vascular cognitive disorder and vascular dementia. Acta Neuropathol. 113, 349–388.
Jellinger, K.A., 2008. Morphologic diagnosis of “vascular dementia” — a critical update. J. Neurol. Sci. 270, 1–12.
Jellinger, K.A., Attems, J., 2006. Prevalence and impact of cerebrovascular pathology in Alzheimer's disease and parkinsonism. Acta Neurol. Scand. 114, 38–46.
Jové, M., Portero-Otín, M., Naudí, A., Ferrer, I., Pamplona, R., 2014. Metabolomics of human brain aging and age-related neurodegenerative diseases. J. Neuropathol. Exp. Neurol. 73, 640–657.
Jung, Y., Wong, E.C., Liu, T.T., 2012. Multiphase pseudocontinuous arterial spin labeling (MP-PCASL) for robust quantification of cerebral blood flow. Magn. Reson. Med. 64, 799–810.
Kamagata, K., Motoi, Y., Hori, M., Suzuki, M., Nakanishi, A., Shimoji, K., Kyougoku, S., Kuwatsuru, R., Sasai, K., Abe, O., Mizuno, Y., Aoki, S., Hattori, N., 2011. Posterior hypoperfusion in Parkinson's disease with and without dementia measured with arterial spin labeling MRI. J. Magn. Reson. Imag. 33, 803–807.
Kannurpatti, S.S., Motes, M.A., Rypma, B., Biswal, B.B., 2011. BOLD signal change: minimizing vascular contri- butions by resting-state-fluctuation-of-amplitude scaling. r H uman B rain M apping 32, 1125–1140.
Kassner, A., Winter, J.D., Poublanc, J., Mikulis, D.J., Crawley, A.P., 2010. Blood-oxygen level dependent MRI measures of cerebrovascular reactivity using a controlled respiratory challenge: reproducibility and gender differences. J. Magn. Reson. Imag. 31, 298–304.
Kim, T., Kim, S.G., 2005. Quantification of cerebral arterial blood volume and cerebral blood flow using MRI with modulation of tissue and vessel (MOTIVE) signals. Magn. Reson. Med. 54, 333–342.
Ko, K.R., Ngai, A.C., Winn, H.R., 1990. Role of adenosine in regulation of regional cerebral blood flow in sensory cortex. Am. J. Physiol. 259, H1703–H1708.
Kwong, K.K., Chesler, D.A., Weisskoff, R.M., Donahue, K.M., Davis, T.L., Ostergaard, L., Campbell, T.A., Rosen, B.R., 1995. MR Perfusion Studies with T1-weighted echo Planar Imaging, vol. 34, pp. 878–887.
Lajoie, I., Nugent, S., Debacker, C., Dyson, K., Tancredi, F.B., Badhwar, A., Belleville, S., Deschaintre, Y., Bellec, P., Doyon, J., Bocti, C., Gauthier, S., Arnold, D., Kergoat, M.-J., Chertkow, H., Monchi, O., Hoge, R.D., 2017. Application of calibrated fMRI in Alzheimer's disease. Neuroimage Clin 15, 348–358.
Lassen, N.A., 1991. Cations as mediators of functional hyperemia in the brain. In: Lassen, N.A., Ingvar, D.H., Raichle, M.E., Friberg, L. (Eds.), Brain Work and Metan Activity: Quantitative Studies with Radioactive Tracers. Munksgaard, Coperhagen, pp. 68–77.
Leenders, K.L., Perani, D., Lammertsma, A.A., Heather, J.D., Buckingham, P., Healy, M.J.R., Gibbs, J.M., Wise, R.J.S., Hatazawa, J., Herold, S., Beaney, R.P., Brooks, D.J., Spinks, T., Rhodes, C., Frackowiak, R.S., Jones, T., 1990. Cerebral blood flow, blood volume and oxygen utilization. Brain 113, 24–47.
Leithner, C., Royl, G., 2013. The oxygen paradox of neurovascular coupling. J. Cerebr. Blood Flow Metabol. 34, 19–29.
Li, K.L., Zhu, X.P., Waterton, J., Jackson, A., 2000. Improved 3D quantitative mapping of blood volume and endothelial permeability in brain tumors. J. Magn. Reson. Imag. 12, 347–357.
Li, W., Watts, L., Long, J., Zhou, W., Shen, Q., Jiang, Z., Li, Y., Duong, T.Q., 2016. Spatiotemporal changes in blood-brain barrier permeability, cerebral blood flow, T2 and diffusion following mild traumatic brain injury. Brain Res. 1646, 53–61.
Liu, P., Li, Y., Pinho, M., Park, D.C., Welch, B.G., Lu, H., 2017. Cerebrovascular reactivity mapping without gas challenges. Neuroimage 146, 320–326.
Lobo, A., Launer, L.J., Fratiglioni, L., Andersen, K., Di Carlo, A., Breteler, M.M., Copeland, J.R., Dartigues, J.F., Jagger, C., Martinez-Lage, J., Soininen, H., Hofman, A., 2000. Prevalence of dementia and major subtypes in Europe: a collaborative study of population-based cohorts. Neurologic Diseases in the Elderly Research Group. Neurology 54, S4–S9.
Lu, H., Golay, X., Pekar, J.J., Van Zijl, P.C.M., 2003. Functional magnetic resonance imaging based on changes in vascular space occupancy. Magn. Reson. Med. 50, 263–274.
Lu, H., Hutchison, J., Xu, F., Rypma, B., 2011a. The relationship between M in “calibrated fMRI” and the physiologic modulators of fMRI. Open Neuroimaging J. 5, 112–119.
Lu, H., Xu, F., Rodrigue, K.M., Kennedy, K.M., Cheng, Y., Flicker, B., Hebrank, A.C., Uh, J., Park, D.C., 2011b. Alterations in cerebral metabolic rate and blood supply across the adult lifespan. Cerebr. Cortex 21, 1426–1434.
Lu, H., Xu, F., Grgac, K., Liu, P., Qin, Q., van Zijl, P., 2012. Calibration and validation of TRUST MRI for the estimation of cerebral blood oxygenation. Magn. Reson. Med. 67, 42–49.
Lulé, D., Ludolph, A.C., Kassubek, J., 2009. MRI-based functional neuroimaging in ALS: an update. Amyotroph Lateral Scler. 10, 258–268.
Maeda, H., Matsumoto, M., Handa, N., Hougaku, H., Ogawa, S., Itoh, T., Tsukamoto, Y., Kamada, T., 1993. Reactivity of cerebral blood flow to carbon dioxide in various types of ischemic cerebrovascular disease: evaluation by the transcranial Doppler method. Stroke 24, 670–675.
Makedonov, I., Chen, J.J., Masellis, M., MacIntosh, B.J., Alzheimer’s Disease Neuroimaging Initiative, 2016. Physiological fluctuations in white matter are increased in Alzheimer's disease and correlate with neuroimaging and cognitive biomarkers. Neurobiol. Aging 37, 12–18.
Mark, C.I., Slessarev, M., Ito, S., Han, J., Fisher, J.A., Pike, G.B., 2010. Precise control of end-tidal carbon dioxide and oxygen improves BOLD and ASL cerebrovascular reactivity measures. Magn. Reson. Med. 64, 749–756.
Marrett, S., Gjedde, A., 1997. Changes of blood flow and oxygen consumption in visual cortex of living humans. Adv. Exp. Med. Biol. 413, 205–208.
Marstrand, J.R., Garde, E., Rostrup, E., Ring, P., Rosenbaum, S., Mortensen, E.L., Larsson, H.B.W., 2002. Cerebral perfusion and cerebrovascular reactivity are reduced in white matter hyperintensities. Stroke 33, 972–976.
McNeill, R., Sare, G.M., Manoharan, M., Testa, H.J., Mann, D.M.A., Neary, D., Snowden, J.S., Varma, A.R., 2006. Accuracy of single-photon emission computed tomography in differentiating frontotemporal dementia from Alzheimer's disease. J. Neurol. Neurosurg. Psychiatry 78, 350–355.
Meyer, J.S., Takashima, S., Terayama, Y., Obara, K., Muramatsu, K., Weathers, S., 1994. CT changes associated with normal aging of the human brain. J. Neurol. Sci. 123, 200–208.
Miao, J., Xu, F., Davis, J., Otte-Höller, I., Verbeek, M.M., Van Nostrand, W.E., 2005. Cerebral microvascular amyloid β protein deposition induces vascular degeneration and neuroinflammation in transgenic mice expressing human vasculotropic mutant amyloid β precursor protein. Am. J. Pathol. 167, 505–515.
Miyakawa, T., Katsuragi, S., Higuchi, Y., Yamashita, K., Kimura, T., Teraoka, K., Ono, T., Ishizuka, K., 1997. Changes of microvessels in the brain with Alzheimer's disease. Ann. N. Y. Acad. Sci. 826, 428–432.
Montagne, A., Barnes, S.R., Sweeney, M.D., Halliday, M.R., Sagare, A.P., Zhao, Z., Toga, A.W., Jacobs, R.E., Liu, C.Y., Amezcua, L., Harrington, M.G., Chui, H.C., Law, M., Zlokovic, B.V., 2015. Blood-brain barrier breakdown in the aging human hippocampus. Neuron 85, 296–302.
Mulligan, S.J., MacVicar, B.A., 2004. Calcium transients in astrocyte endfeet cause cerebrovascular constrictions. Nature 431, 195–199.
Mullins, R., Reiter, D., Kapogiannis, D., 2018. Magnetic resonance spectroscopy reveals abnormalities of glucose metabolism in the Alzheimer's brain. Annals of Clinical and Translational Neurology 5, 262–272.
Newberg, A.B., Alavi, A., 2010. PET in the Aging Brain. Elsevier Health Sciences.
Newman, E.J., 2009. Prevalence and Diagnosis of Parkinson's Disease: a Community Study.

Nobili, F., Copello, F., Buffoni, F., Vitali, P., Girtler, N., Bordoni, C., Safaie-Semnani, E., Mariani, G., Rodriguez, G., 2001. Regional cerebral blood flow and prognostic evaluation in Alzheimer's disease. Dement. Geriatr. Cognit. Disord. 12, 89–97.
Ogawa, S., Lee, T.M., Kay, A.R., Tank, D.W., 1990. Brain magnetic resonance imaging with contrast dependent on blood oxygenation. Proc. Natl. Acad. Sci. U. S. A 87, 9868–9872.
Ostergaard, L., Weisskoff, R.M., Chesler, D.A., Gyldensted, C., Rosen, B.R., 1996. High resolution measurement of cerebral blood flow using intravascular tracer bolus passages. Part I: mathematical approach and statistical analysis. Magn. Reson. Med. 36, 715–725.
Park, L., Zhou, P., Pitstick, R., Capone, C., Anrather, J., Norris, E.H., Younkin, L., Younkin, S., Carlson, G., McEwen, B.S., Iadecola, C., 2008. Nox2-derived radicals contribute to neurovascular and behavioral dysfunction in mice overexpressing the amyloid precursor protein. Proc. Natl. Acad. Sci. U. S. A 105, 1347–1352.
Parkes, L.M., 2005. Quantification of cerebral perfusion using arterial spin labeling: two-compartment models. J. Magn. Reson. Imag. 22, 732–736.
Paulson, O.B., Hasselbalch, S.G., Rostrup, E., Knudsen, G.M., Pelligrino, D., 2010. Cerebral blood flow response to functional activation. J. Cerebr. Blood Flow Metabol. 30, 2–14.
Peca, S., McCreary, C.R., Donaldson, E., Kumarpillai, G., Shobha, N., Sanchez, K., Charlton, A., Steinback, C.D., Beaudin, A.E., Flück, D., Pillay, N., Fick, G.H., Poulin, M.J., Frayne, R., Goodyear, B.G., Smith, E.E., 2013. Neurovascular decoupling is associated with severity of cerebral amyloid angiopathy. Neurology 81, 1659–1665.
Peisker, T., Bartoš, A., Skoda, O., Ibrahim, I., Kalvach, P., 2010. Impact of aging on cerebral vasoregulation and parenchymal integrity. J. Neurol. Sci. 299, 112–115.
Pezzini, A., Del Zotto, E., Volonghi, I., Giossi, A., Costa, P., Padovani, A., 2009. Cerebral amyloid angiopathy: a common cause of cerebral hemorrhage. Curr. Med. Chem. 16, 2498–2513.
Pezzoli, S., Cagnin, A., Bandmann, O., Venneri, A., 2017. Structural and functional neuroimaging of visual hallucinations in Lewy body disease: a systematic literature review. Brain Sci. 7. https://doi.org/10.3390/brainsci7070084.
Pillai, J.J., Mikulis, D.J., 2015. Cerebrovascular reactivity mapping: an evolving standard for clinical functional imaging. AJNR Am. J. Neuroradiol 36, 7–13.
Pluta, R., Jolkkonen, J., Cuzzocrea, S., Pedata, F., Cechetto, D., Popa-Wagner, A., 2011. Cognitive impairment with vascular impairment and degeneration. Curr. Neurovascular Res. 8, 342–350.
Poublanc, J., Han, J.S., Mandell, D.M., Conklin, J., Stainsby, J.A., Fisher, J.A., Mikulis, D.J., Crawley, A.P., 2013. Vascular steal explains early paradoxical blood oxygen level-dependent cerebrovascular response in brain regions with delayed arterial transit times. Cerebrovasc. Dis. Extra 3, 55–64.
Poublanc, J., Crawley, A.P., Sobczyk, O., Montandon, G., Sam, K., Mandell, D.M., Dufort, P., Venkatraghavan, L., Duffin, J., Mikulis, D.J., Fisher, J.A., 2015. Measuring cerebrovascular reactivity: the dynamic response to a step hypercapnic stimulus. J. Cerebr. Blood Flow Metabol. 35, 1746–1756.
Poulin, M.J., Liang, P.J., Robbins, P.A., 1996. Dynamics of the cerebral blood flow response to step changes in end-tidal PCO2 and PO2 in humans. J. Appl. Physiol. 81, 1084–1095.
Power, J.H.T., Barnes, O.L., Chegini, F., 2016. Lewy bodies and the mechanisms of neuronal cell death in Parkinson's disease and dementia with Lewy bodies. Brain Pathol. 27, 3–12.
Prince, M., Bryce, R., Albanese, E., Wimo, A., Ribeiro, W., Ferri, C.P., 2013. The global prevalence of dementia: a systematic review and metaanalysis. Alzheimers. Dement 9, 63–75 e2.
Qin, Q., Grgac, K., van Zijl, P.C.M., 2010. Determination of whole-brain oxygen extraction fractions by fast measurement of blood T2 in the jugular vein. Magn. Reson. Med. 65, 471–479.
Qiu, M., Maguire, P.R., Arora, J., Planeta-Wilson, B., Weinzimmer, D., Wang, J., Wang, Y., Kim, H.S., Rajeevan, N., Huang, Y., Carson, R., Constable, R.T., 2010. Arterial transit time effects in pulsed arterial spin labeling CBF mapping: insight from a PET and MR study in normal human subjects. Magn. Reson. Med. 63, 374–384.
Raz, L., Knoefel, J., Bhaskar, K., 2016. The neuropathology and cerebrovascular mechanisms of dementia. J. Cerebr. Blood Flow Metabol. 36, 172–186.
Reijmer, Y.D., Fotiadis, P., Charidimou, A., van Veluw, S.J., Xiong, L., Riley, G.A., Martinez-Ramirez, S., Schwab, K., Viswanathan, A., Gurol, M.E., Greenberg, S.M., 2017. Relationship between white matter connectivity loss and cortical thinning in cerebral amyloid angiopathy. Hum. Brain Mapp. https://doi.org/10.1002/hbm.23629.
Rémy, F., Mirrashed, F., Campbell, B., Richter, W., 2004. Mental calculation impairment in Alzheimer's disease: a functional magnetic resonance imaging study. Neurosci. Lett. 358, 25–28.
Restom, K., Bangen, K.J., Bondi, M.W., Perthen, J.E., Liu, T.T., 2007. Cerebral blood flow and BOLD responses to a memory encoding task: a comparison between healthy young and elderly adults. Neuroimage 37, 430–439.
Richiardi, J., Monsch, A.U., Haas, T., Barkhof, F., Van de Ville, D., Radü, E.W., Kressig, R.W., Haller, S., 2015. Altered cerebrovascular reactivity velocity in mild cognitive impairment and Alzheimer's disease. Neurobiol. Aging 36, 33–41.
Roh, J.H., Lee, J.-H., 2014. Recent updates on subcortical ischemic vascular dementia. J. Stroke Cerebrovasc. Dis. 16, 18–26.
Roher, A.E., Lowenson, J.D., Clarke, S., Woods, A.S., Cotter, R.J., Gowing, E., Ball, M.J., 1993. beta-Amyloid-(1-42) is a major component of cerebrovascular amyloid deposits: implications for the pathology of Alzheimer disease. Proc. Natl. Acad. Sci. Unit. States Am. 90, 10836–10840.
Roquet, D., Sourty, M., Botzung, A., Armspach, J.-P., Blanc, F., 2016. Brain perfusion in dementia with Lewy bodies and Alzheimer's disease: an arterial spin labeling MRI study on prodromal and mild dementia stages. Alzheimer's Res. Ther. 8. https://doi.org/10.1186/s13195-016-0196-8.
Rosenberg, G.A., 2014. Blood-brain barrier permeability in aging and Alzheimer's disease. J Prev Alzheimers Dis 1, 138–139.
Rossini, P.M., Rossi, S., Babiloni, C., Polich, J., 2007. Clinical neurophysiology of aging brain: from normal aging to neurodegeneration. Prog. Neurobiol. 83, 375–400.
Rosso, S.M., 2003. Frontotemporal dementia in The Netherlands: patient characteristics and prevalence estimates from a population-based study. Brain 126, 2016–2022.
Roy, C.S., Sherrington, C.S., 1890. On the regulation of the blood supply of the brain. J. Physiol. 11, 85–105.
Sakoh, M., Røhl, L., Gyldensted, C., Gjedde, A., Ostergaard, L., 2000. Cerebral blood flow and blood volume measured by magnetic resonance imaging bolus tracking after acute stroke in pigs: comparison with [(15)O]H(2)O positron emission tomography. Stroke 31, 1958–1964.
Salat, D.H., 2004. Thinning of the cerebral cortex in aging. Cerebr. Cortex 14, 721–730.
Sato, N., Morishita, R., 2013. Roles of vascular and metabolic components in cognitive dysfunction of Alzheimer disease: short- and long-term modification by non-genetic risk factors. Front. Aging Neurosci. 5, 64.
Schmitz, B., Wang, X., Barker, P.B., Pilatus, U., Bronzlik, P., Dadak, M., Kahl, K.G., Lanfermann, H., Ding, X.-Q., 2018. Effects of aging on the human brain: a proton and phosphorus MR spectroscopy study at 3T. J. Neuroimaging. https://doi.org/10.1111/jon.12514.
Schroeter, M.L., Schmiedel, O., von Cramon, D.Y., 2004. Spontaneous low-frequency oscillations decline in the aging brain. J. Cerebr. Blood Flow Metabol. 24, 1183–1191.
Schuff, N., Matsumoto, S., Kmiecik, J., Studholme, C., Du, A., Ezekiel, F., Miller, B.L., Kramer, J.H., Jagust, W.J., Chui, H.C., Weiner, M.W., 2009. Cerebral blood flow in ischemic vascular dementia and Alzheimer's disease, measured by arterial spin-labeling magnetic resonance imaging. Alzheimers. Dement 5, 454–462.
Schulte, P.A., Perera, F.P., 2012. Molecular Epidemiology: Principles and Practices. Academic Press.
Shulman, R.G., Hyder, F., Rothman, D.L., 2001. Cerebral energetics and the glycogen shunt: neurochemical basis of functional imaging. Proc. Natl. Acad. Sci. Unit. States Am. 98, 6417–6422.
Siegal, T., Rubinstein, R., Tzuk-Shina, T., Gomori, J.M., 1997. Utility of relative cerebral blood volume mapping derived from perfusion magnetic resonance imaging in the routine follow up of brain tumors. J. Neurosurg. 86, 22–27.
Siegfried, K., 1993. The cholinergic hypothesis of Alzheimer's disease. Eur. Neuropsychopharmacol 3, 170–171.
Slessarev, M., Han, J., Mardimae, A., Prisman, E., Preiss, D., Volgyesi, G., Ansel, C., Duffin, J., Fisher, J.A., 2007. Prospective targeting and control of end-tidal CO2 and O2 concentrations. J. Physiol. 581, 1207–1219.
Sobczyk, O., Battisti-Charbonney, A., Fierstra, J., Mandell, D.M., Poublanc, J., Crawley, A.P., Mikulis, D.J., Duffin, J., Fisher, J.A., 2014. A conceptual model for CO_2-induced redistribution of cerebral blood flow with experimental confirmation using BOLD MRI. Neuroimage 92, 56–68.
Sourbron, S., Ingrisch, M., Siefert, A., Reiser, M., Herrmann, K., 2009. Quantification of cerebral blood flow, cerebral blood volume, and blood-brain-barrier leakage with DCE-MRI. Magn. Reson. Med. 62, 205–217.
Spees, W.M., Yablonskiy, D.A., Oswood, M.C., Ackerman, J.J., 2001. Water proton MR properties of human blood at 1.5 Tesla: magnetic susceptibility, T1, T2, T2*, and non-Lorentzian signal behavior. Magn. Reson. Med. 45, 533–542.
Sperling, R.A., Bates, J.F., Chua, E.F., Cocchiarella, A.J., Rentz, D.M., Rosen, B.R., Schacter, D.L., Albert, M.S., 2003. fMRI studies of associative encoding in young and elderly controls and mild Alzheimer's disease. J. Neurol. Neurosurg. Psychiatry 74, 44–50.
Starr, J.M., Farrall, A.J., Armitage, P., McGurn, B., Wardlaw, J., 2009. Blood–brain barrier permeability in Alzheimer's disease: a case–control MRI study. Psychiatr. Res. Neuroimaging 171, 232–241.
Stefanovic, B., Pike, G.B., 2005. Venous refocusing for volume estimation: VERVE functional magnetic resonance imaging. Magn. Reson. Med. 53, 339–347.
Steketee, R.M.E., Bron, E.E., Meijboom, R., Houston, G.C., Klein, S., Mutsaerts, H.J.M.M., Mendez Orellana, C.P., de Jong, F.J., van Swieten, J.C., van der Lugt, A., Smits, M., 2016. Early-stage differentiation between presenile Alzheimer's disease and frontotemporal dementia using arterial spin labeling MRI. Eur. Radiol. 26, 244–253.
Stout, J.N., Adalsteinsson, E., Rosen, B.R., Bolar, D.S., 2018. Functional oxygen extraction fraction (OEF) imaging with turbo gradient spin echo QUIXOTIC (Turbo QUIXOTIC). Magn. Reson. Med. 79, 2713–2723.
Strittmatter, W.J., Saunders, A.M., Schmechel, D., Pericak-Vance, M., Enghild, J., Salvesen, G.S., Roses, A.D., 1993. Apolipoprotein E: high-avidity binding to beta-amyloid and increased frequency of type 4 allele in late-onset familial Alzheimer disease. Proc. Natl. Acad. Sci. U. S. A 90, 1977–1981.
Suri, S., Mackay, C.E., Kelly, M.E., Germuska, M., Tunbridge, E.M., Frisoni, G.B., Matthews, P.M., Ebmeier, K.P., Bulte, D.P., Filippini, N., 2014. Reduced cerebrovascular reactivity in young adults carrying the APOE epsilon4 allele. Alzheimers. Dement. https://doi.org/10.1016/j.jalz.2014.05.1755.
Tak, S., Wang, D.J.J., Polimeni, J.R., Yan, L., Chen, J.J., 2014. Dynamic and static contributions of the cerebrovasculature to the resting-state BOLD signal. Neuroimage 84, 672–680.
Tancredi, F.B., Hoge, R.D., 2013. Comparison of cerebral vascular reactivity measures obtained using breath-holding and CO2 inhalation. J. Cerebr. Blood Flow Metabol. 33, 1066–1074.
Tarumi, T., Ayaz Khan, M., Liu, J., Tseng, B.Y., Parker, R., Riley, J., Tinajero, C., Zhang, R., 2014. Cerebral hemodynamics in normal aging: central artery stiffness,

wave reflection, and pressure pulsatility. J. Cerebr. Blood Flow Metabol. 34, 971–978.
Teeuwisse, W.M., Schmid, S., Ghariq, E., Veer, I.M., van Osch, M.J., 2014. Time-encoded pseudocontinuous arterial spin labeling: basic properties and timing strategies for human applications. Magn. Reson. Med. Epub ahead of print. https://doi.org/10.1002/mrm.25083.
Telischak, N.A., Detre, J.A., Zaharchuk, G., 2014. Arterial spin labeling MRI: clinical applications in the brain. J. Magn. Reson. Imag. 41, 1165–1180.
Thal, D.R., von Arnim, C.A.F., Griffin, W.S.T., Mrak, R.E., Walker, L., Attems, J., Arzberger, T., 2015. Frontotemporal lobar degeneration FTLD-tau: preclinical lesions, vascular, and Alzheimer-related co-pathologies. J. Neural. Transm. 122, 1007–1018.
Théberge, J., 2008. Perfusion magnetic resonance imaging in psychiatry. Top. Magn. Reson. Imag. 19, 111–130.
Thomas, B.P., Liu, P., Park, D.C., van Osch, M.J., Lu, H., 2014. Cerebrovascular reactivity in the brain white matter: magnitude, temporal characteristics, and age effects. J. Cerebr. Blood Flow Metabol. 34, 242–247.
Thomas, B.P., Sheng, M., Tseng, B.Y., Tarumi, T., Martin-Cook, K., Womack, K.B., Cullum, M.C., Levine, B.D., Zhang, R., Lu, H., 2017. Reduced global brain metabolism but maintained vascular function in amnestic mild cognitive impairment. J. Cerebr. Blood Flow Metabol. 37, 1508–1516.
Thulborn, K.R., Waterton, J.C., Radda, G.K., 1981. Proton imaging for in vivo blood flow and oxygen consumption measurements. J. Magn. Reson. 45, 188–191.
Toescu, E.C., Verkhratsky, A., 2004. Ca2+ and mitochondria as substrates for deficits in synaptic plasticity in normal brain ageing. J. Cell Mol. Med. 8, 181–190.
Tofts, P.S., Kermode, A.G., 1991. Measurement of the blood-brain barrier permeability and leakage space using dynamic MR imaging. 1. Fundamental concepts 17, 357–367.
Tosun, D., Schuff, N., Jagust, W., Weiner, M.W., Alzheimer''s Disease Neuroimaging Initiative, 2016. Discriminative power of arterial spin labeling magnetic resonance imaging and 18F-fluorodeoxyglucose positron emission tomography changes for amyloid-β-positive subjects in the Alzheimer's disease continuum. Neurodegener. Dis. 16, 87–94.
Turner, M.R., Modo, M., 2010. Advances in the application of MRI to amyotrophic lateral sclerosis. Expert Opin. Med. Diagn. 4, 483–496.
van de Haar, H.J., Burgmans, S., Jansen, J.F.A., van Osch, M.J.P., van Buchem, M.A., Muller, M., Hofman, P.A.M., Verhey, F.R.J., Backes, W.H., 2016. Blood-brain barrier leakage in patients with early alzheimer disease. Radiology 281, 527–535.
Van Den Eeden, S.K., Tanner, C.M., Bernstein, A.L., Fross, R.D., Leimpeter, A., Bloch, D.A., Nelson, L.M., 2003. Incidence of Parkinson's disease: variation by age, gender, and race/ethnicity. Am. J. Epidemiol. 157, 1015–1022.
van der Zande, F.H., Hofman, P.A., Backes, W.H., 2005. Mapping hypercapnia-induced cerebrovascular reactivity using BOLD MRI. Neuroradiology 47, 114–120.
van Osch, J.P., M, van Osch, M.J.P., Lu, H., 2011. Arterial spin labeling perfusion MRI in alzheimers disease. Curr. Med. Imag. Rev. 7, 62–72.
Varma, A.R., Adams, W., Lloyd, J.J., Carson, K.J., Snowden, J.S., Neary, D., Jackson, A., Testa, H.J., 1999. Patterns of regional cerebral blood flow change on SPET and regional atrophy on MRI in Alzheimer's disease, vascular dementia and frontotemporal dementia. Nucl. Med. Commun. 20, 469.
Varma, A.R., Adams, W., Lloyd, J.J., 2002. … atrophy on MRI and regional cerebral blood flow change on SPECT in young onset patients with Alzheimer's disease, frontotemporal dementia and vascular dementia. Acta Neurol.
Verclytte, S., Lopes, R., Lenfant, P., Rollin, A., Semah, F., Leclerc, X., Pasquier, F., Delmaire, C., 2016. Cerebral hypoperfusion and hypometabolism detected by arterial spin labeling MRI and FDG-PET in early-onset Alzheimer's disease. J. Neuroimaging 26, 207–212.
Vicenzini, E., Ricciardi, M.C., Altieri, M., Puccinelli, F., Bonaffini, N., Di Piero, V., Lenzi, G.L., 2007. Cerebrovascular reactivity in degenerative and vascular dementia: a transcranial Doppler study. Eur. Neurol. 58, 84–89.
Viticchi, G., Falsetti, L., Vernieri, F., Altamura, C., Bartolini, M., Luzzi, S., Provinciali, L., Silvestrini, M., 2012. Vascular predictors of cognitive decline in patients with mild cognitive impairment. Neurobiol. Aging 33, 1127 e1–9.
Wang, Z., 2014. Characterizing early Alzheimer's disease and disease progression using hippocampal volume and arterial spin labeling perfusion MRI. J. Alzheimers. Dis. 42 (Suppl. 4), S495–S502.
Wang, J., Licht, D.J., Jahng, G.H., Liu, C.S., Rubin, J.T., Haselgrove, J., Zimmerman, R.A., Detre, J.A., 2003. Pediatric perfusion imaging using pulsed arterial spin labeling. J. Magn. Reson. Imag. 18, 404–413.
Wang, D.J.J., Liebeskind, D.S., Qiao, J.X., Gunther, M., Pope, W.B., Saver, J.L., Salamon, N., Alger, J.R., 2013. Multi-delay multi-parametric arterial spin-labeled perfusion MRI in acute ischemic stroke – comparison with dynamic susceptibility contrast enhanced perfusion imaging. Presented at the Int Soc Magn Reson Med.
Wang, R., Yu, S., Alger, J.R., Zuo, Z., Chen, J., Wang, R., An, J., Wang, B., Zhao, J., Xue, R., Wang, D.J., 2014. Multi-delay arterial spin labeling perfusion MRI in moyamoya disease–comparison with CT perfusion imaging. Eur. Radiol. 24, 1135–1144.
Weller, R.O., Massey, A., Newman, T.A., Hutchings, M., Kuo, Y.M., Roher, A.E., 1998. Cerebral amyloid angiopathy: amyloid beta accumulates in putative interstitial fluid drainage pathways in Alzheimer's disease. Am. J. Pathol. 153, 725–733.
Whitworth, H.B., Whitworth, J.A., 2014. Managing Cognitive Issues: in Parkinson's Disease and Other Lewy Body Disorders (Whitworths of Arizona).
Wierenga, C.E., Dev, S.I., Shin, D.D., Clark, L.R., Bangen, K.J., Jak, A.J., Rissman, R.A., Liu, T.T., Salmon, D.P., Bondi, M.W., 2012. Effect of mild cognitive impairment and APOE genotype on resting cerebral blood flow and its association with cognition. J. Cerebr. Blood Flow Metabol. 32, 1589–1599.
Wierenga, C.E., Hays, C.C., Zlatar, Z.Z., 2014. Cerebral blood flow measured by arterial spin labeling MRI as a preclinical marker of Alzheimer's disease. J. Alzheimers. Dis. 42 (Suppl. 4), S411–S419.
Williams, R.J., Goodyear, B.G., Peca, S., McCreary, C.R., Frayne, R., Smith, E.E., Pike, G.B., 2017. Identification of neurovascular changes associated with cerebral amyloid angiopathy from subject-specific hemodynamic response functions. J. Cerebr. Blood Flow Metabol. 271678X17691056.
Wintermark, M., Sesay, M., Barbier, E., Borbély, K., Dillon, W.P., Eastwood, J.D., Glenn, T.C., Grandin, C.B., Pedraza, S., Soustiel, J.-F., Nariai, T., Zaharchuk, G., Caillé, J.-M., Dousset, V., Yonas, H., 2005. Comparative overview of brain perfusion imaging techniques. Stroke 36, e83–99.
Wirestam, R., Ryding, E., Lindgren, A., Geijer, B., Ostergaard, L., Andersson, L., Holtås, S., Ståhlberg, F., 2000. Regional cerebral blood flow distributions in normal volunteers: dynamic susceptibility contrast MRI compared with 99mTc-HMPAO SPECT. J. Comput. Assist. Tomogr. 24, 526–530.
Wolk, D., Mancuso, L., Rao, H., Detre, J., 2011. Rest and task-related arterial spin labeling MRI in MCI. Alzheimers. Dement. 7, S229.
Wong, E.C., Buxton, R.B., Frank, L.R., 1997. Implementation of quantitative perfusion imaging techniques for functional brain mapping using pulsed arterial spin labeling. NMR Biomed. 10, 237–249.
Wong, E.C., Buxton, R.B., Frank, L.R., 1999. Quantitative perfusion imaging using arterial spin labeling. Neuroimaging Clin. 9, 333–342.
Wu, C.W., Liu, H.-L., Chen, J.-H., Yang, Y., 2010. Effects of CBV, CBF, and blood-brain barrier permeability on accuracy of PASL and VASO measurement. Magn. Reson. Med. 63, 601–608.
Xekardaki, A., Rodriguez, C., Montandon, M.-L., Toma, S., Tombeur, E., Herrmann, F.R., Zekry, D., Lovblad, K.-O., Barkhof, F., Giannakopoulos, P., Haller, S., 2015. Arterial spin labeling may contribute to the prediction of cognitive deterioration in healthy elderly individuals. Radiology 274, 490–499.
Yang, G., Zhang, Y., Elizabeth Ross, M., Iadecola, C., 2003. Attenuation of activity-induced increases in cerebellar blood flow in mice lacking neuronal nitric oxide synthase. Am. J. Physiol. Heart Circ. Physiol. 285, H298–H304.
Yankner, B.A., Lu, T., Loerch, P., 2008. The aging brain. Annu. Rev. Pathol. 3, 41–66.
Ye, F.Q., Berman, K.F., Ellmore, T., Esposito, G., van Horn, J.D., Yang, Y., Duyn, J., Smith, A.M., Frank, J.A., Weinberger, D.R., McLaughlin, A.C., 2000. H215O PET validation of steady-state arterial spin tagging cerebral blood flow measurements in humans. Magn. Reson. Med. 44, 450–456.
Yezhuvath, U.S., Uh, J., Cheng, Y., Martin-Cook, K., Weiner, M., Diaz-Arrastia, R., van Osch, M., Lu, H., 2012. Forebrain-dominant deficit in cerebrovascular reactivity in Alzheimer's disease. Neurobiol. Aging 33, 75–82.
Yin, J., Sun, H., Yang, J., Guo, Q., 2014. Automated detection of the arterial input function using normalized cut clustering to determine cerebral perfusion by dynamic susceptibility contrast-magnetic resonance imaging. J. Magn. Reson. Imag. 41, 1071–1078.
Zago, S., Poletti, B., Morelli, C., Doretti, A., Silani, V., 2011. Amyotrophic lateral sclerosis and frontotemporal dementia (ALS-FTD). Arch. Ital. Biol. 149, 39–56.
Zaitsu, Y., Kudo, K., Terae, S., Yazu, R., Ishizaka, K., Fujima, N., Tha, K.K., Haacke, E.M., Sasaki, M., Shirato, H., 2011. Mapping of cerebral oxygen extraction fraction changes with susceptibility-weighted phase imaging. Radiology 261, 930–936.
Zazulia, A.R., Videen, T.O., Morris, J.C., Powers, W.J., 2010. Autoregulation of cerebral blood flow to changes in arterial pressure in mild Alzheimer's disease. J. Cerebr. Blood Flow Metabol. 30, 1883–1889.
Zhang, J.H., Badaut, J., Tang, J., Obenaus, A., Hartman, R., Pearce, W.J., 2012. The vascular neural network–a new paradigm in stroke pathophysiology. Nat. Rev. Neurol. 8, 711–716.
Zhang, J., Liu, T., Gupta, A., Spincemaille, P., Nguyen, T.D., Wang, Y., 2014. Quantitative mapping of cerebral metabolic rate of oxygen (CMRO2) using quantitative susceptibility mapping (QSM). Magn. Reson. Med. 74, 945–952.
Zhang, J., Zhou, D., Nguyen, T.D., Spincemaille, P., Gupta, A., Wang, Y., 2016. Cerebral metabolic rate of oxygen (CMRO2) mapping with hyperventilation challenge using quantitative susceptibility mapping (QSM). Magn. Reson. Med. 77, 1762–1773.
Zhong, W., Cruickshanks, K.J., Schubert, C.R., Carlsson, C.M., Chappell, R.J., Klein, B.E.K., Klein, R., Acher, C.W., 2014. Pulse wave velocity and cognitive function in older adults. Alzheimer Dis. Assoc. Disord. 28, 44–49.
Zlokovic, B.V., 2008. The blood-brain barrier in health and chronic neurodegenerative disorders. Neuron 57, 178–201.
Zonta, M., Angulo, M.C., Gobbo, S., Rosengarten, B., Hossmann, K.A., Pozzan, T., Carmignoto, G., 2003. Neuron-to-astrocyte signaling is central to the dynamic control of brain microcirculation. Nat. Neurosci. 6, 43–50.
Zou, J.-X., Wang, M.-J., Lei, X.-J., Chen, X.-G., 2014. 3.0 T MRI arterial spin labeling and magnetic resonance spectroscopy technology in the application of Alzheimer's disease. Exp. Gerontol. 60, 31–36.